# Notch signalling regulates epibranchial placode patterning and segregation

Li Wang[1], Junjie Xie[1], Haoran Zhang[1], Long Hin Tsang[1], Sze Lan Tsang[1], Eike-Benjamin Braune[2], Urban Lendahl[2] and Mai Har Sham[1,#]

[1]School of Biomedical Sciences, LKS Faculty of Medicine, The University of Hong Kong, Pokfulam, Hong Kong SAR, China;
[2]Department of Cell and Molecular Biology, Karolinska Institutet, Stockholm, Sweden.

[#]Correspondence should be addressed to:
Professor Mai Har Sham, 3/F Laboratory Block, Faculty of Medicine Building, The University of Hong Kong, 21 Sassoon Road, Pokfulam, Hong Kong SAR, China.
Tel: +852 3917 9195
Fax: +852 2855 1254

Email: mhsham@hku.hk

**Key words:**
epibranchial placode, pharyngeal ectoderm, Notch signalling, N1ICD, Rbpj

**Summary statement:**
Notch signaling regulates the rostral-caudal patterning and commitment of the epibranchial placodal region into repeated *Vgll2+/Irx5+* and *Sox2+/Fgf3+/Etv5+* domains along the pharyngeal clefts, leading to the formation of individual placodes.

**Abstract**

Epibranchial placodes are the geniculate, petrosal and nodose placodes which generate parts of cranial nerves VII, IX and X, respectively. How the three spatially separated placodes are derived from the common posterior placodal area is poorly understood. Here, we reveal that the broad posterior placode area is first patterned into a *Vgll2+/Irx5+* rostral domain and a *Sox2+/Fgf3+/Etv5+* caudal domain relative to the first pharyngeal cleft. This initial rostral and caudal patterning is then sequentially repeated along each pharyngeal cleft for each epibranchial placode. The caudal domains give rise to the neuronal and non-neuronal cells in the placode, while the rostral domains are previously unrecognized structures, serving as spacers between the final placodes. Notch signalling regulates the balance between the rostral and caudal domains: high levels of Notch signalling expand the caudal domain at the expense of the rostral domain, whereas loss of Notch signalling produces the converse phenotype. Collectively, these data unravel a new patterning principle for the early phases of epibranchial placode development and a role for Notch signalling in orchestrating epibranchial placode segregation and differentiation.

## Introduction

Cranial placodes are transient ectodermal thickenings that give rise to specialized sensory organs and ganglia of the cephalic peripheral nervous system. Cranial placodes arise from a common pre-placodal region, which separates into anterior, intermediate and posterior placodal areas (PPAs), before segregating into discrete individual placodes (Saint-Jeannet and Moody, 2014; Schlosser, 2010; Schlosser and Ahrens, 2004; Streit, 2004). The epibranchial placodes are named based on their locations dorsal-caudal to the pharyngeal (branchial) clefts and stem from the PPA. They give rise to the viscerosensory neurons of the distal ganglia of the facial (VIII), glossopharyngeal (IX) and vagal (X) cranial nerves to innervate various visceral organs to collect sensory information (Baker and Bronner-Fraser, 2001).

The PPA emerges on the ectodermal surface adjacent to the neural plate, at the level of the caudal hindbrain and rostral to the first somite. The PPA contains a common otic-epibranchial precursor domain that expresses *Pax2, Sox2* and *Sox3* and is recognizable at around embryonic day 8.5 (E8.5) (4-6 somite stage, ss) in mouse and chick embryos (Fig. 1A) (Chen and Streit, 2013). The otic territory and the lateral epibranchial territory, a contiguous region of thickened epithelium on the proximal pharyngeal ectoderm, become molecularly distinct and gradually separated by E9.0 (14-16 ss). At around E9.25 (20ss), the otic placode invaginates to form the otic cup, and the epibranchial territory is split into a rostral geniculate domain, and a caudal domain which will become the future petrosal and nodose placodes (Ishii et al., 2001; Ladher et al., 2010; Washausen and Knabe, 2017). By E9.5 (24-27 ss), the otic vesicle is formed, and the three pairs of epibranchial placodes are confined to the dorsal-caudal position of their respective pharyngeal clefts (Fig. 1A). While it has long been established that the *Neurog2*-expressing domain of the epibranchial placodes generates neurons of the cranial nerves, it was recently observed that each epibranchial placode also harbours a non-neuronal cell population, characterized by combined *Sox2* and *Fgf3* expression (Zhang et al., 2017).

During the early stages of placode development, the PPA contains multipotent precursors that acquire different placodal fates. For the epibranchial placodes, it remains unclear whether the PPA contains predetermined precursors that are

intermingled and subsequently segregate into distinct placodes, or whether specification of regional placodal fates occurs later when uncommitted cells respond to local signalling factors. A key feature of epibranchial placodes is their coordinated development with the pharyngeal arches (PA). The three pairs of epibranchial placodes are intimately associated with the pharyngeal arch segmentation process, during which the pharyngeal ectoderm fuses with the endoderm forming clefts on the surface and the pocket-like pouches in the endoderm (Graham, 2003). The morphological changes and cell movements during the formation of PAs may separate the pool of epibranchial placodal precursors into their final locations. *Pax2, Sox2* and *Sox3* are initially broadly expressed in the PPA and retained in the placodal cells, but down-regulated in the 'interplacodal' regions (Ishii et al., 2001; Tripathi et al., 2009; Washausen and Knabe, 2017). It has been suggested that apoptosis in the 'interplacodal' regions and proliferation of placodal cells could promote the physical segregation of the three discrete epibranchial placodes (Washausen and Knabe, 2013; Washausen and Knabe, 2017; Washausen and Knabe, 2018; Washausen et al., 2005). The mechanisms underlying the segregation of the placodal precursors into specific epibranchial placodes however remain unclear.

A number of signalling mechanisms are implicated in epibranchial placode differentiation, including BMP, Wnt, FGF and Notch signalling (Begbie et al., 2002; Begbie et al., 1999; Freter et al., 2008; Koo et al., 2005; Kriebitz et al., 2009; Litsiou et al., 2005; McCarroll and Nechiporuk, 2013; Urness et al., 2010). The Notch signalling pathway is an evolutionarily conserved cell-cell communication system that regulates cell differentiation and homeostasis in most organs (Siebel and Lendahl, 2017). In mammals, there are four receptors (Notch1-4) and five ligands (Jag1-2 and Dll1,3,4). Interaction between transmembrane Notch ligands and receptors on juxtaposed cells initiates signalling in the receptor-expressing cell. Ligand interaction leads to sequential proteolytic cleavage of the Notch receptor, which liberates its C-terminal domain (referred as the Notch intracellular domain, NICD). NICD translocates to the nucleus to form a ternary transcriptional complex with the DNA-binding protein CSL (RBP-j κ) and MAML. When Notch signalling is not activated, in the absence of NICD, CSL acts as repressor by interacting with co-repressors, but switches to an activator when NICD contacts CSL to displace the co-repressors with co-activators

(Bray, 2016; Siebel and Lendahl, 2017). Notch receptors are also modified by Fringe proteins, which are glycosyltransferases, and Fringe-mediated extensions of O-linked fucose-adducts on the Notch receptor extracellular domain alter the receptor's preference for signalling via Dll and Jagged types of ligand (for review see (Harvey and Haltiwanger, 2018). Notch signalling in conjunction with Eya1 has recently been shown to be important for the differentiation to the neuronal (*Neurog2*+) and non-neuronal (*Sox2*+ *Fgf3*+) fates in epibranchial placodes (Zhang et al., 2017).

In this report, we address the early steps of epibranchial placode development to elucidate how cell specification occurs from the PPA to the segregation of the spatially separated geniculate, petrosal and nodose epibranchial placodes. We identify an early patterning event, with the appearance of a rostral *Vgll2+/Irx5*+ domain and a caudal *Sox2+/Fgf3+/Etv5*+ domain located on opposite sides of the first pharyngeal cleft. This rostral-caudal patterning is then repeated along the second and third clefts, which precede the formation of the geniculate, petrosal and nodose epibranchial placodes. Notch signalling coordinates the balance between the rostral and caudal domains: high levels of Notch promote the caudal program, while loss of Notch signalling activity conversely expands the rostral territory. In conclusion, these data provide novel insights into the genesis of epibranchial placodes and define a role for Notch signalling in epibranchial patterning and segregation.

## Results

### A *Pax2*+ posterior placodal area gives rise to multiple placodal and epithelial cell types

*Pax2* is one of the earliest specific makers for the PPA (Baker et al., 2008; McCarroll et al., 2012; Ohyama and Groves, 2004a; Streit, 2002). To follow the fate of the *Pax2*+ PPA cells we performed lineage tracing experiments using *Pax2-Cre* (Ohyama and Groves, 2004a) and *Rosa26-EYFP* (Srinivas et al., 2001) or *Rosa26-lacZ* (Soriano, 1999) mice. At E8.5, *lacZ* reporter expression was observed at the PPA, covering a lateral surface caudal to the first pharyngeal arch (PA1) and rostral to the first somite (Fig. 1B); a distribution consistent with previous data from both mouse and chick embryos (Wright and Mansour, 2003). At this stage, other *Pax2*+ cells can also be

found in the brain and the migrating neural crest within the first pharyngeal arch. At E9.5, *lacZ* reporter expression in the pharyngeal region covered a broad domain encompassing the otic vesicle and proximal pharyngeal ectoderm (Fig. 1C). Analysis of serial coronal sections of E9.5 *Pax2-Cre;Rosa*$^{EYFP}$ embryos revealed that the otic vesicle, the geniculate and petrosal placodal cells as well as delaminated Islet1+ neuroblasts were labelled by EYFP (Fig. 1 E-I). Notably, at this stage *Pax2* expression was confined to the otic vesicle (Fig. 1E') and *Pax2* was no longer expressed in the epibranchial epithelial cells. The serial section analysis showed that the proximal pharyngeal epithelial cells (Fig. 1E-H), but not the cells covering the distal pharyngeal arch, were EYFP+ (Fig. 1I), indicating that the whole proximal pharyngeal ectodermal area is derived from the *Pax2*+ PPA. Similar results were also obtained using *Sox2CreERT2;Rosa*$^{EYFP}$ mice, showing that a broad range of pharyngeal epithelial cells were derived from the PPA (Fig. S1 and Fig. 5 A,C,E).

Within the *Pax2*-labelled proximal pharyngeal ectoderm, the epibranchial placodes could be identified as thickened epithelial cells, while the surrounding interplacodal pharyngeal ectoderm thinned out and adopted a surface epithelial morphology (Muller and O'Rahilly, 1988; Tripathi et al., 2009; Washausen et al., 2005). We further examined the epibranchial placodal area using *Sox2*, a placodal marker gene, *Irx5* which is expressed in PPA (Feijoo et al., 2009; Glavic et al., 2004), and acetylated tubulin, which marks motile cilia on ciliated cells. We found that the epibranchial placodal cells expressing *Sox2* were marked with acetylated tubulin (Fig. 1 J, K). Conversely, the epithelial cells marked by *Irx5* (indicated by EGFP in *Irx5*$^{EGFP/+}$ embryos) had a much lower density of acetylated tubulin (Fig. 1K). The Sox2+ epibranchial placodal cells also expressed cyclin D1 (Fig. 1M), suggesting that these cells were proliferative. We further examined cell proliferation and apoptosis by PH3 and TUNEL analysis, respectively (Fig. 1N,O and Fig. S3). Our data confirmed previous findings that apoptosis could be detected in the pharyngeal clefts, while epithelial regions were proliferative (Washausen et al., 2005). These results are consistent with the notion that *Pax2*+ PPA progenitors gave rise to both otic and epibranchial placodes, as well as their surrounding non-neural cells (as indicated in Fig. 1A) (Ohyama and Groves, 2004b; Streit, 2002).

**Stepwise regionalization of epibranchial placode and proximal pharyngeal ectoderm**

We next addressed the question of how the pool of *Pax2*+ PPA progenitors may segregate into three discrete epibranchial placodes as well as interplacodal pharyngeal ectodermal cells. We first investigated the spatiotemporal patterning of the epibranchial placodes from E8.5 to E9.5 using a series of placodal and pharyngeal markers including *Eya1/Six1* (placodal progenitor markers); *Neurog2* (the earliest pre-neural marker in epibranchial placode (Fode et al., 1998); *Sox2* (essential for epibranchial neural competence) (Gou et al., 2018; Tripathi et al., 2009); *Irx5* (expressed in PPA) (Feijoo et al., 2009; Glavic et al., 2004); *Vestigial-like2* (*Vgll2*, expressed in pharyngeal region) (Chen et al., 2017; Johnson et al., 2011); *Fgf3* and the FGF downstream target *Etv5* (critical for pharyngeal morphogenesis) (Urness et al., 2011).

At around E8.5, before the appearance of the first pharyngeal cleft (c1), *Eya1* was detected specifically in the PPA (Fig. 2A). At this stage, *Vgll2* expression first appeared in the emerging PA1 and *Fgf3* was expressed in the hindbrain, while neither of them was detected in the epibranchial placodal region (Fig. 2A) (see also (Zhang et al., 2017)). At around E8.75, c1 became morphologically visible while c2 (second pharyngeal cleft) was not yet formed. *Eya1* was expressed in the expanded PPA, spanning from the rostral part of the first cleft, caudally extending to the first somite, dorsally to the otic placodal region and ventrally to the proximal PA (Fig. 2A). *Vgll2* was expressed rostrally of c1 and at the presumptive c2, its expression in PA1 (beyond the epibranchial placodal region) was expanded, whereas *Fgf3* was first detected at a position caudal of c1 (Fig. 2A). At around E9.0, c2 could be morphologically identified ventral to the otic pit. *Eya1* continued to label the broad epibranchial placodal region, while a second *Fgf3*+ domain appeared (Fig. 2A). The locations of the Fgf3+ domains were caudal and complementary to the Vgll2+ domains. At E9.5, all three clefts were formed. *Eya1* expression persisted in the whole otic-epibranchial placodal region, with distinctive expression in the otic vesicle and geniculate, petrosal and nodose placodes, and a lower level of expression at the interplacodal pharyngeal epithelium. Three *Vgll2*+ and three *Fgf3*+ domains were detected at the proximal pharyngeal arches in a complementary manner (Fig. 2A). *Sox2* expression appeared earlier than *Fgf3* in the PPA at E8.5 and was gradually confined to the caudal of each cleft until E9.5 (Fig.

2A,B). *Neurog2* expression was not detected until E8.75, when it was found specifically at the dorsal of each *Fgf3*+ domains (Fig. 2A) (see also (Zhang et al., 2017)). As illustrated in Fig. 1A, “rostral” and “caudal” domains are in relation to the pharyngeal clefts.

To examine gene expression patterns across the embryo, coronal sections of embryos from E8.5 to E9.5 were analysed with different markers. *Six1*, as one of the pan-placodal markers, was expressed early at the placodal ectoderm, and also in the pharyngeal endodermal, mesenchymal and mesodermal cells at E8.5 (Fig. 2B). Later, in line with the development of pharyngeal arches from E8.75-E9.5, three clefts and pouches appeared sequentially. *Six1* expression was broadly detected at the epibranchial placodes and proximal PA ectodermal cells (Fig. 2B). Sox2 was initially expressed broadly along the PPA ectoderm at E8.5, but it was gradually restricted to domains caudal to each cleft from E9.0 (Fig. 2B). Etv5 (also called Erm), a downstream target of FGF signalling (Roehl and Nusslein-Volhard, 2001), was expressed in the pharyngeal ectoderm, endoderm and mesenchymal cells. From E9.0, Etv5 was expressed at positions caudal to each of the developing pharyngeal clefts (Fig. 2B). In contrast, Irx5 was highly expressed in the pharyngeal mesoderm, but by E9.5 its expression was observed in the ectodermal region rostral to each cleft (Fig. 2B). Similarly, *Vgll2* was expressed only at rostral domain of each cleft as shown in coronal sections (Fig. 2B), complementary to the Sox2+/Etv5+ regions along the proximal ectoderm.

In summary, our results suggest that, after separation from the otic territory, the *Eya1*+/*Six1*+ epibranchial placodal area expanded caudally as the pharyngeal arches were generated. From E8.5 onwards, accompanying the appearance of each pharyngeal cleft, a *Vgll2*+/*Irx5*+ domain (rostral to each cleft), and a *Sox2*+/*Etv5*+ domain (caudal to each cleft) appeared in a complementary manner, finally resulting in three repeated, intercalated rostral and caudal domains within the broad proximal pharyngeal ectoderm (Fig. 2C). Meanwhile, the dorsal-caudal neurogenic patches, which delaminate neurons to contribute to epibranchial ganglia, and the *Fgf3*+ caudal patches were both differentiated from the caudal *Sox2*+ pre-neural domains (Zhang et al., 2017). The specification of rostral domains served as segregations for the three

discrete caudal domains, providing an intriguing morphological explanation for the metameric patterning of geniculate, petrosal and nodose placodes (Fig. 2C).

**Regionalized expression of Notch factors during epibranchial specification**

Notch signalling has been shown to regulate placodal cell differentiation in olfactory, otic and other placodes. In order to determine whether Notch signalling is involved during the individualization of epibranchial placodes from the broader PPA, the spatiotemporal expression patterns of Notch signalling factors were examined. The Notch ligand *Jag1* and the Notch target gene *Hey1* were confined to the c1 and c2 regions at E9.5 (Fig. 3A). *Jag1* was expressed early within the PPA region at around E8.5 (Fig. S2 and data not shown) and restricted to otic placode and cleft regions at E9.5 (Fig. 3B) (Zhang et al., 2017). *Hey1* expression could be detected from E8.75 and later restricted to the caudal domains (Fig. 3B and Fig. S2). *HeyL* was detected in both the rostral and caudal domains (Fig. 3A). *Jag2* expression appeared at around E8.75 at the rostral region of c1 (Fig. 3B), and *Jag2* was expressed at the rostral regions of c1 and c2 at E9.5 (Fig. 3A,B), illustrating a rostral domain-restricted expression pattern. *Dll1* expression first appeared at both rostral and caudal regions at E9.0 (Fig. S2). However, the expression of *Dll1* was specifically restricted to the dorsal neurogenic regions at E9.5 (Fig. 3A). Another Hes family member, *Hes6*, was specifically expressed in the dorsal neurogenic domain (Fig. 3A). *Dll3* was not detected at the PPA at E9.5 (data not shown). *Hes1, which* was reported to function in PA development but not in epibranchial placode (Kameda et al., 2013; van Bueren et al., 2010), was contiguously expressed at the whole pharyngeal ectoderm (Fig. S2 and data not shown).

Among the three *Fringe* (*Fng*) genes, which encode glycosyltransferases that modulate Notch receptors by glycosylation, *Rfng* was not expressed in the epibranchial territory, whereas *Mfng* was restricted to the dorsal-caudal neurogenic domain as well as migrating neuroblasts (Fig. 3A). *Lfng* was detected at the dorsal-caudal neurogenic domain, with weak expression at the ventral-caudal domains as well (Fig. 3A). We have previously reported the expression of Notch1 in the proximal pharyngeal ectoderm (Zhang et al., 2017). At E9.5, Notch1 was highly expressed at the caudal ectoderm relative to each cleft, and also in the mesenchyme (Fig. 3B), in line with a previous study (Williams et al., 1995).

In summary, these data show that the rostral and caudal domains are endowed with distinct expression patterns for genes in the Notch signalling pathway (summarized in Fig. 3C), suggesting a role for Notch signalling in the differentiation and segregation of the epibranchial placodes from the PPA.

**Notch signalling mediates the regional specification of proximal pharyngeal ectoderm**

To investigate the effect of Notch signalling on patterning the proximal pharyngeal ectoderm along the rostrocaudal and dorsoventral axes, the expression of regional markers was examined in *Pax2-Cre;Rosa*$^{N1\text{-}IC}$ embryos, where N1ICD is activated in the PPA using the *Pax2-Cre* driver from E8.5 to E9.5, or in *Actin-Cre;Rbpj*$^{flox/flox}$ embryos, where *Rbpj* was deleted by *Actin-Cre*, leading to a loss of the canonical Notch signalling activity from the zygotic stage. While *Vgll2* was normally localized at the rostral domains in wildtype (WT) E9.5 embryos (Fig. 4A,B), expression of *Vgll2* was specifically lost in the pharyngeal ectoderm of *Pax2-Cre;Rosa*$^{N1\text{-}IC}$ embryos (Fig. 4B). Interestingly, in *Actin-Cre;Rbpj*$^{flox/flox}$ embryos expression of *Vgll2* expanded into the caudal domains of cleft1 and cleft2, covering the entire proximal PA ectoderm (Fig. 4A,B). The *Vgll2* expansion was not observed in the mandibular arch of *Rbpj* mutant, in keeping with the presence of Notch signalling factors in the PPA but not in mandibular arch (Fig.3). The effect of Notch signalling on caudal domain genes was opposite compared with the rostral domain genes. Expression of *Fgf3* was elevated when Notch activity was high, whereas the *Fgf3*+ caudal domains were greatly reduced in the *Rbpj* mutant embryos (Fig. 4A). The expression of *Etv5*, which is one of the downstream targets of FGF signalling and as such an indicator of FGF activity, was upregulated in *Pax2-Cre;Rosa*$^{N1\text{-}IC}$ embryos while down-regulated in *Actin-Cre;Rbpj*$^{flox/flox}$ embryos (Fig. 4A,B). This indicates that although canonical Notch signalling was not required for the initiation of *Etv5* and *Fgf3* expression, it was essential for their maintenance, and that FGF activity was also under the regulation of Notch signalling. Moreover, the expression of *Neurog2*, one of the earliest markers for neural precursors in epibranchial placodes, was inhibited when N1ICD was activated (Fig. 4A), which is consistent with the function of Notch signalling in inhibiting neural differentiation in multiple neural systems. The expression of *Neurog2* was slightly reduced when canonical Notch activity was inhibited (Fig. 4A).

To investigate the distribution of Notch ligands and target genes that may be involved in the rostral-caudal patterning process, we examined the expression of *Jag1*, *Jag2*, *Dll1*, *HeyL*, *Hey1* and *Hes6* in response to activation or loss of Notch signalling. The expression of *HeyL* and *Hey1* was elevated when N1ICD was overexpressed in pharyngeal ectoderm and downregulated in *Actin-Cre;Rbpj*$^{flox/flox}$ embryos (Fig. 4A), suggesting that they are Notch targets in this context. In contrast, the expression of *Hes6*, as well as of *Neurog2*, was lost in *Pax2-Cre;Rosa*$^{N1\text{-}IC}$ embryos, while slightly reduced in *Actin-Cre;Rbpj*$^{flox/flox}$ embryos (Fig. 4A). Notably, we found that the expression of *Jag2* and *Dll1* was inhibited, while the expression of *Jag1* was enhanced by elevated Notch signalling (Fig. 4A).

To characterize the rostral and caudal cell fates in the Notch mutants, we examined the distribution of acetylated tubulin, which was highly expressed in caudal cells in *WT* embryos. When Notch was activated, acetylated tubulin was broadly expressed in the whole epibranchial territory (Fig. 4B). In contrast, inhibition of canonical Notch in the *Actin-Cre;Rbpj*$^{flox/flox}$ embryos led to decreased expression of acetylated tubulin in the pharyngeal ectoderm, whereas the endodermal expression remained similar to what was observed in *WT* embryos (Fig. 4B). In summary, these observations demonstrate that the rostral *Vgll2* expression was inhibited while the caudal *Fgf3, Etv5* and acetylated tubulin expression was expanded when Notch activity was elevated (Fig. 4C). Conversely, low level of canonical Notch activity through inhibition of *Rbpj* resulted in expansion of rostral markers into caudal domains, while the expression of caudal genes was significantly reduced (Fig. 4C).

**A cell autonomous role of Notch signalling in regulating the rostrocaudal specification of proximal pharyngeal ectoderm**

We next addressed whether Notch signalling exerted a cell autonomous role in specifying the proximal pharyngeal ectoderm. To this end, we used *Sox2CreERT2* activation to label epithelial cell clones in a mosaic fashion. By tamoxifen induction at E7.5 and harvesting the *Sox2CreERT2;Rosa*$^{EYFP}$ embryos at E9.5, EYFP+ cells could be found in both rostral and caudal domains (Fig. 5A,C). This suggests that both the *Sox2*-negative rostral and the *Sox2*-positive caudal cells originated from early *Sox2*+ progenitors, consistent with our results shown in Fig. 1 using *Pax2-Cre*. We activated N1ICD in the PPA cells of *Sox2creERT2*;*Rosa*$^{N1\text{-}IC}$ embryos by tamoxifen induction at

E7.5, and cells with induced N1ICD expression would be identified by expression of *GFP* which was linked to *N1ICD* via an IRES element. Some *GFP*+ cells were found at the rostral domains in E9.5 *Sox2creERT2;Rosa*$^{N1\text{-}IC}$ embryos (Fig. 5B,D). Strikingly, these *GFP*+ cells were highly *Sox2*+ (Fig. 5B') and expressed high levels of acetylated tubulin (Fig. 5D'), indicating a caudal cell identity. Expression of Sox2 and acetylated tubulin was confined to the rostral cells exhibiting *GFP* (and by inference *N1ICD*) activity but was not observed in surrounding GFP-negative cells, indicating a cell autonomous role of Notch signalling in activating and/or maintaining the *Sox2* expression and multi-ciliated morphology. However, while the effect on *Sox2* and acetylated tubulin expression was confined to the *N1ICD-GFP*+ cells in the rostral domain, we observed that cells immediately adjacent to the *N1ICD-GFP*+ cells were *Neurog2*+ (Fig. 5E-H). Collectively, these observations indicate that high Notch activity in rostrally located cells can induce a caudal fate switch, and that adjacent cells as a consequence take on *Neurog2* expression.

## Discussion

This study lays out the process of stepwise individualization of epibranchial placodes from the broader *Pax2*+ posterior placodal area (PPA). Firstly, the *Pax2*-expressing PPA gave rise to not only otic and epibranchial placodes, but also to proximal pharyngeal surface ectoderm. Secondly, the epibranchial territory of the PPA encompassed the proximal pharyngeal ectoderm and expanded caudally from the first pharyngeal arch as the second and third pharyngeal arches were generated. Subsequently, within the broad *Eya1+/Six1*+ region, accompanying the appearance of each pharyngeal cleft, a *Vgll2+/Irx5*+ domain and a *Sox2+/Fgf3+/Etv5*+ domain appeared at the rostral and caudal positions of each cleft, respectively. The sequential patterning resulted in intercalated rostral and caudal repeating domains along the epibranchial region. In parallel, the *Neurog2*+ neurogenic patches were induced at the dorsal edge of each caudal domain and gradually downregulated *Sox2* expression, whereas the ventral portions remained as *Sox2+/Fgf3*+ (Zhang et al., 2017). Ultimately, the regionalization of the proximal pharyngeal ectoderm in a rostrocaudal sequence led to the appearance of three discrete *Neurog2*+ epibranchial placodes (summarized in Fig. 6). Notch signalling contributed to the subdivision of *Pax2*+ PPA both

rostrocaudally and dorsoventrally: high levels of Notch activity led to expanded expression of caudal genes into rostral domains and inhibited neural differentiation in the dorsal-caudal placodal region.

**Regional specification and patterning of epibranchial placodes**

Lineage tracing by *Pax2-Cre* and *Sox2-CreERT2* showed that epibranchial precursors gave rise to a wide range of derivatives, including not only epibranchial neurons, but also the rostral and caudal proximal pharyngeal ectodermal cells, supporting an origin from the placodal region for these ectodermal derivatives. Lineage tracing by *Sox2-CreERT2;Rosa*$^{EYFP}$ with tamoxifen injected at E7.5 and E8.5 revealed that both the rostral and caudal cells were labelled by EYFP at E9.5. In contrast, the caudal cells were Sox2-negative, suggesting that the rostral non-neural cells lost the Sox2 expression at around E9.5 (Fig. 1 and Fig. S1). Moreover, the rostral *Vgll2+/Irx5+* cells showed a thin and cuboidal morphology versus a thickened ciliated morphology for the ventral-caudal *Sox2+/Fgf3+/Etv5+* cells (Fig. 1), further underscoring their distinct fates.

Our data provided evidence for regional patterning of epibranchial placodes, through which the placodal (caudal) cells and the interplacodal (rostral) cells were specified into distinct fates with different transcriptional profiles and cellular morphology. In line with this notion, the interplacodal cells exhibited a loss of placodal signature revealed by reduced *Sox2* and *Pax2* expression, accompanied by a local gain of *Vgll2* expression (Fig. 2). Secondly, interplacodal and placodal cells became morphologically different (Fig. 1). This is in agreement with previous observation that the entire branchial region is initially covered with thick ectoderm which becomes thinner from around E8.75 (10ss), leaving thicker cells in the epibranchial placodes (Baker and Bronner-Fraser, 2001; Verwoerd and van Oostrom, 1979). Our observations are also consistent with previous studies in chick, mouse and human embryos, where the epibranchial placodes arose from more extended areas of thickened branchial ectoderm (Abu-Elmagd et al., 2001; Baker and Bronner-Fraser, 2000; D'Amico-Martel and Noden, 1983; Muller and O'Rahilly, 1988; Washausen and Knabe, 2013; Washausen and Knabe, 2017; Washausen et al., 2005). Moreover, our

data corroborate a previous report of thickened morphology in the posterior placodal area in the Northern treeshrew (*Tupaia belangeri)* (Washausen et al., 2005).

**The cellular mechanism for the individualization of epibranchial placodes**

How the geniculate, petrosal and nodose placodes are physically segregated from each other is a long-standing question. Two possible scenarios include local sorting-out of intermingled pre-defined progenitors or regional cell fate changes of multipotent precursors in response to exposure to regional signals (Breau and Schneider-Maunoury, 2014; McCabe and Bronner-Fraser, 2009). The results presented here support a scheme where multipotent precursors are regionally specified into epibranchial placodal cells as well as non-placodal cells. In line with this, before the individual epibranchial placodes become molecularly distinct from surrounding ectoderm, *Eya1, Six1* and *Sox2* were expressed in the broad contiguous proximal pharyngeal ectoderm (Fig. 2). Shortly thereafter, the expression of Sox2 began to progressively become restricted to smaller subdomains that located at the caudal side of each cleft, whereas the expression of *Vgll2* began to appear in complementary rostral subdomains, thereby subdividing the broad proximal pharyngeal ectoderm by establishing distinct *Sox2*+ and *Vgll2*+ regions. *Neurog2* expression was induced at the dorsal edge of the *Sox2*+ caudal subdomains, making epibranchial placodes molecularly distinct from other proximal pharyngeal ectodermal cells. Notably, from E8.5 onwards, the expression of *Sox2* and *Vgll2* was likely to be mutually exclusive, and *Sox2*+ and *Vgll2*+ cells were morphologically distinct, suggesting that the two different cell fates are regionally specified, rather than sorted out from intermingled precursors. Moreover, lineage tracing analysis by *Sox2CreERT2;Rosa*$^{EYFP}$ revealed that both rostral and caudal cells originated from *Sox2*+ progenitors, further supporting regional specification from a common pool of *Sox2*+ progenitors.

**Patterning of the proximal pharyngeal epithelia and pharyngeal arch development**

Previous studies of pharyngeal patterning focused on the anteroposterior organization of the *Hox* code, which provided identities for the PAs, except for the *Hox*-free PA1 (Grammatopoulos et al., 2000). For each PA, the proximodistal organization was

characterized by the *Dlx* code (Minoux and Rijli, 2010). In this study, we showed that in the proximal pharyngeal region, the surface epithelium was not homogeneous, but distinctly patterned along the rostrocaudal axis. As such, for each proximal PA, the anterior half was covered with *Sox2+/Fgf3+/Etv5+* ectodermal cells, whereas the posterior half was *Vgll2+/Irx5+*. Notably, the rostrocaudal patterning of placodal epithelial cells was observed from the region rostral to the first pharyngeal cleft while the rest of the mandibular arch was not included. Furthermore, the specification of rostrocaudal epithelial identity and the process of pharyngeal segmentation were temporally coordinated. It was previously suggested that an additional physical boundary was required to ensure the stable segregation of cells with distinct identities (Schlosser, 2006), and the formation of pharyngeal clefts, which fused with pharyngeal pouches to form pharyngeal segments, may serve as such a boundary between the rostral and caudal domains of the proximal pharyngeal surface ectoderm. It is possible that the rostrocaudal epithelial specification might instruct the segmentation process, and loss of caudal domain factors, such as *Sox3* and FGF signalling in mice indeed led to defective segmentation (Rizzoti and Lovell-Badge, 2007; Trokovic et al., 2003). Once in contact with the pharyngeal cleft, the pharyngeal pouch would produce a BMP signal to further induce neurogenesis in each caudal domain (Begbie et al., 1999).

**The role of Notch in specifying rostrocaudal and dorsoventral regionalization of the proximal pharyngeal ectoderm**

Our data point to an important role for Notch signalling in controlling the development of the rostral and caudal domains. Notch activation enhanced the differentiation of *Pax2+* precursors into *Sox2+/Fgf3+/Etv5+* caudal cells, at the expense of *Vgll2+/Irx5+* rostral cells and *Neurog2+* dorsal-caudal pre-neural cells. Conversely, inhibition of canonical Notch signalling by deletion of *Rbpj* led to differentiation of *Pax2+* precursors to *Vgll2+/Irx5+* rostral cells instead of *Sox2+/Fgf3+/Etv5+* caudal cells. In the *Rbpj* knockout mutant embryos, expression of *Neurog2* was reduced (Fig. 4A), which is consistent with the requirement of Notch signalling for induction of the pre-neural fate (de la Pompa et al., 1997). In line with promotion of a caudal fate, high Notch signalling favoured differentiation of acetylated tubulin+ ciliated cells at the expense of the flattened cells and neurons. This provides evidence for a role of Notch signalling in the early phases of epibranchial placode differentiation and extends previous reports on

a role for *Dll1* in generation of petrosal and nodose ganglia (Begbie et al., 2002; de la Pompa et al., 1997) and in segregation of neuronal and non-neuronal cells in the epibranchial placodes (Zhang et al., 2017).

The mosaic expression of *N1ICD* in the *Sox2-CreERT2* embryos, where *N1ICD-GFP*-expressing cells were *Sox2*+ and acetylated tubulin+, revealed a cell autonomous role for N1ICD. Interestingly, cells adjacent to the *N1ICD-GFP*-expressing cells exhibited an altered fate, with elevated *Neurog2* expression, which likely is a secondary effect of the changed fate in the *N1ICD-GFP*-expressing cells. This constitutes a classical example of lateral inhibition or specification, a mechanism ensuring segregation of distinct fates in a field of initially homogenous cells. Lateral inhibition regulated by Notch signalling has been extensively demonstrated in *Drosophila* and in a few situations in mammals, such as inner ear development (see (Sjoqvist and Andersson, 2019)for review).

Genes in the Notch signalling pathway showed complex expression patterns during epibranchial differentiation and in the rostral and caudal domains, notably with regard to Notch ligand and *Fngs* expression (summarized in Fig. 3C). The subdivision into a *Dll1/Fngs* versus a *Jag1* expressing territory is very similar to what is observed during dorsoventral patterning and specification of the developing spinal cord (Marklund et al., 2010), and likely regulating how Notch signalling is deployed in segregating and maintaining the identities of the rostral and dorsal domains. Modification of Notch receptors by Fngs enhances Dll1-Notch signalling, while repressing Jag1-Notch signalling (Harvey and Haltiwanger, 2018; Siebel and Lendahl, 2017). As for the developing spinal cord (Marklund et al., 2010), this may lead to intradomain Notch signalling in the caudal neural domain, while signalling is abrogated across the boundary to the rostral domain. The *Dll1/Fngs* and *Jag1* domain-specific expression patterns observed here are in contrast to, for example, the situation in the *Drosophila* wing blade, where the presence of *Ser/Fng* and *Dll1*-expressing domains ensure inter-domain Notch activation only at the boundary (in the wing blade), but not within the different domains (Wu and Rao, 1999).

How Notch signalling controls the upregulation of certain genes (*Sox2, Fgf3* and *Etv5*) while repressing other genes (*Neurog2, Vgll2* and *Irx5)* (summarized in Fig. 6C) is not

fully understood. Repression of gene activity may involve Notch downstream genes of the *Hes* and *Hey* family, where *Hey1* is expressed in all domains, while *Hes6* expression is confined to the caudal neural domain. Hes genes have been shown to antagonize expression of proneural genes (Ohtsuka et al., 1999). There are indeed a number of potential Hes-binding sites in or near the *Vgll2* and *Irx5* genes, but it is not yet experimentally established whether Hes proteins dynamically bind to these sites. Upregulation may be a direct consequence of activation via the NICD/MAML/CSL ternary complex, but in chromatin immunoprecipitation (ChIP) experiments in cell lines, CSL binding to potential binding sites near the Sox2 and Fgf3 genes was not observed (data not shown), indicating that the effect may be indirect. In conclusion, this study shed new light onto the early epibranchial specification by providing evidence for a non-neural developmental trajectory from the epibranchial precursors and a role for Notch in this process.

## Materials and Methods

### Experimental Animals

The mouse lines used in this study include wildtype C57BL/6N, *Rosa*$^{N1\text{-}IC}$ (Murtaugh et al., 2003); *Rbpj*$^{flox/flox}$ (Han et al., 2002); *Rosa*$^{EYFP}$ (Srinivas et al., 2001); *Rosa*$^{LacZ}$ (Soriano, 1999); *Irx5*$^{EGFP/+}$ (Li et al., 2014); *Pax2-cre* (Xu et al., 2002) and *Sox2-creERT2* (Arnold et al., 2011). Mice were maintained on a C57BL/6N background and housed at the Laboratory Animal Unit, the University of Hong Kong. Genotyping was conducted by PCR using primers listed in Table S1. To activate Cre activity in *Sox2creERT2* embryos, tamoxifen (Sigma-Aldrich, Cat#06734) was dissolved in corn oil (20mg/ml) and administered by intraperitoneal injection to pregnant females (0.1mg/g body weight) at E7.5 to E9.5. For each stage and each genotype, at least 3 embryos were collected for further analysis. All mouse experiments were approved by the University of Hong Kong animal research ethics committee (CULATR No. 4357-17).

### Riboprobe labelling

Plasmids with target cDNA sequences were obtained from other laboratories or cloned in this study as shown in Table S2. The cDNA plasmids were linearized with restriction

enzymes (summarized in Table S3), separated on 1% low melting agarose gel and purified. DNA samples were dissolved in DEPC $H_2O$, 1µg purified DNA was used for reverse transcription and Dig-labelling (11093274910, Sigma-Aldrich). Labelled RNA probes were precipitated in ethanol, air-dried, dissolved in DEPC $H_2O$ and stored at -80°C.

**Whole-mount X-gal staining and *in situ* hybridization**

The activity of β-galactosidase in *Rosa*$^{lacZ}$ reporter was analysed by X-gal staining as described in (Kwan et al., 2001). Briefly, embryos were fixed in 0.2% glutaraldehyde, 1.5% formaldehyde at 4°C for 30 to 90 min. The embryos were then washed and stained in dark in 1 mg/ml X-gal (7240906, Sigma-Aldrich) at room temperature for 1hr. For *in situ* hybridization, embryos from E8.5 to E9.5 were harvested in cold DEPC PBS and fixed in 4% paraformaldehyde at 4°C overnight. Embryos were then dehydrated with a graded series of DEPC methanol/PBST solution, stored at -20°C or proceed to the next steps. Before performing *in situ* hybridization, the embryos were rehydrated, treated with protease K (P8811, Sigma-Aldrich) and then post-fixed with 4% paraformaldehyde, 0.2% glutaraldehyde and washed in PBST. Embryos were pre-hybridized by incubating at 55-65°C for 3hrs, DIG-labeled riboprobes were then added into the hybridization mix and incubated at 55-65°C overnight. After hybridization, embryos were washed in hybridization mix/MABT solution, then blocked with 10% blocking reagent and 20% heat-inactivated horse serum. Anti-Digoxigenin-alkaline phosphatase (11093274910, Sigma-Aldrich) was added to the embryos and incubated overnight at 4°C. After washing for 24 hr, embryos were immersed in BM purple substrate (Roche) until clear signal were detected. The reaction was stopped by washing in PBST and post-fixation with 4% paraformaldehyde.

**Histology and immunohistochemistry**

Mouse embryos were fixed in 4% paraformaldehyde at 4°C for 1 hr or overnight, according to the requirement of specific antibodies. After fixation, embryos were washed in PBS, incubated in 15% sucrose overnight at 4°C, then transferred to gelatin solution and incubated at 37°C. Embryos were embedded in gelatin block, cut to suitable size and stored at -80°C before 10 µm sections were prepared.

For immunostaining, histological sections were blocked with 10% horse serum in PBS at room temperature for 1hr, primary antibodies were applied to the sections and

incubated at 4°C overnight. Sections were then washed and incubated with fluorescent-linked secondary antibodies for 1h at room temperature. At this step, DAPI (D9542, Sigma) was co-stained with secondary antibodies. Histological slides were then washed in PBS before mounted with mounting medium (Vectashield). Images were captured using an Olympus fluorescence microscope (BX51). At least 3 different sections from three different embryos were stained with each primary antibody. The primary and secondary antibodies used were summarized in Table S4.

**TUNEL assay**

Histological sections were incubated in permeabilisation solution (0.1% Triton X-100, 0.1% sodium citrate) for 2 min on ice, then washed twice with PBS. Slides were incubated with TUNEL reaction mixture (1684795910, Roche; enzyme solution and label solution at 1:9 ratio) at 37°C for 30 min, followed by three washes in PBS. Sections were mounted in mounting medium (Vectashield).

**Acknowledgements**

We thank C.C. Hui (Toronto, Canada) for kindly providing the Irx5-EGFP mice, F. Costantini (New York, USA) for the Etv5 probe, Yuchen Liu, Ka Kui Tong and Karl So for technical assistance.

**Competing interests**

The authors of this manuscript declare no conflict of interests.

**Funding**

This work was supported by a research grant from the Hong Kong Research Grants Council (RGC GRF 17113415) to MHS. WL was supported by a Hong Kong PhD Fellowship. UL was funded by the Swedish Research Council and the Swedish Cancer Society.

## References


**Abu-Elmagd, M., Ishii, Y., Cheung, M., Rex, M., Le Rouedec, D. and Scotting, P. J.** (2001). cSox3 expression and neurogenesis in the epibranchial placodes. *Dev Biol* **237**, 258-269.

**Arnold, K., Sarkar, A., Yram, M. A., Polo, J. M., Bronson, R., Sengupta, S., Seandel, M., Geijsen, N. and Hochedlinger, K.** (2011). Sox2(+) adult stem and progenitor cells are important for tissue regeneration and survival of mice. *Cell Stem Cell* **9**, 317-329.

**Baker, C. V. and Bronner-Fraser, M.** (2000). Establishing neuronal identity in vertebrate neurogenic placodes. *Development* **127**, 3045-3056.

**Baker, C. V. and Bronner-Fraser, M.** (2001). Vertebrate cranial placodes I. Embryonic induction. *Dev Biol* **232**, 1-61.

**Baker, C. V., O'Neill, P. and McCole, R. B.** (2008). Lateral line, otic and epibranchial placodes: developmental and evolutionary links? *J Exp Zool B Mol Dev Evol* **310**, 370-383.

**Begbie, J., Ballivet, M. and Graham, A.** (2002). Early steps in the production of sensory neurons by the neurogenic placodes. *Mol Cell Neurosci* **21**, 502-511.

**Begbie, J., Brunet, J. F., Rubenstein, J. L. and Graham, A.** (1999). Induction of the epibranchial placodes. *Development* **126**, 895-902.

**Bray, S. J.** (2016). Notch signalling in context. *Nat Rev Mol Cell Biol* **17**, 722-735.

**Breau, M. A. and Schneider-Maunoury, S.** (2014). Mechanisms of cranial placode assembly. *Int J Dev Biol* **58**, 9-19.

**Chen, J. and Streit, A.** (2013). Induction of the inner ear: stepwise specification of otic fate from multipotent progenitors. *Hear Res* **297**, 3-12.

**Chen, J., Tambalo, M., Barembaum, M., Ranganathan, R., Simoes-Costa, M., Bronner, M. E. and Streit, A.** (2017). A systems-level approach reveals new gene regulatory modules in the developing ear. *Development* **144**, 1531-1543.

**D'Amico-Martel, A. and Noden, D. M.** (1983). Contributions of placodal and neural crest cells to avian cranial peripheral ganglia. *Am J Anat* **166**, 445-468.

**de la Pompa, J. L., Wakeham, A., Correia, K. M., Samper, E., Brown, S., Aguilera, R. J., Nakano, T., Honjo, T., Mak, T. W., Rossant, J., et al.** (1997). Conservation of the Notch signalling pathway in mammalian neurogenesis. *Development* **124**, 1139-1148.

**Feijoo, C. G., Saldias, M. P., De la Paz, J. F., Gomez-Skarmeta, J. L. and Allende, M. L.** (2009). Formation of posterior cranial placode derivatives requires the Iroquois transcription factor irx4a. *Mol Cell Neurosci* **40**, 328-337.

**Fode, C., Gradwohl, G., Morin, X., Dierich, A., LeMeur, M., Goridis, C. and Guillemot, F.** (1998). The bHLH protein NEUROGENIN 2 is a determination factor for epibranchial placode-derived sensory neurons. *Neuron* **20**, 483-494.

**Freter, S., Muta, Y., Mak, S. S., Rinkwitz, S. and Ladher, R. K.** (2008). Progressive restriction of otic fate: the role of FGF and Wnt in resolving inner ear potential. *Development* **135**, 3415-3424.

**Glavic, A., Maris Honoré, S., Gloria Feijóo, C., Bastidas, F., Allende, M. L. and Mayor, R.** (2004). Role of BMP signaling and the homeoprotein iroquois in the specification of the cranial placodal field. *Developmental Biology* **272**, 89-103.

**Gou, Y., Guo, J., Maulding, K. and Riley, B. B.** (2018). sox2 and sox3 cooperate to regulate otic/epibranchial placode induction in zebrafish. *Dev Biol* **435**, 84-95.

**Graham, A.** (2003). Development of the pharyngeal arches. *Am J Med Genet A* **119A**, 251-256.

**Grammatopoulos, G. A., Bell, E., Toole, L., Lumsden, A. and Tucker, A. S.** (2000). Homeotic transformation of branchial arch identity after Hoxa2 overexpression. *Development* **127**, 5355-5365.

**Han, H., Tanigaki, K., Yamamoto, N., Kuroda, K., Yoshimoto, M., Nakahata, T., Ikuta, K. and Honjo, T.** (2002). Inducible gene knockout of transcription factor recombination signal binding protein-J reveals its essential role in T versus B lineage decision. *Int Immunol* **14**, 637-645.

**Harvey, B. M. and Haltiwanger, R. S.** (2018). Regulation of Notch Function by O-Glycosylation. *Adv Exp Med Biol* **1066**, 59-78.

**Ishii, Y., Abu-Elmagd, M. and Scotting, P. J.** (2001). Sox3 expression defines a common primordium for the epibranchial placodes in chick. *Dev Biol* **236**, 344-353.

**Johnson, C. W., Hernandez-Lagunas, L., Feng, W., Melvin, V. S., Williams, T. and Artinger, K. B.** (2011). Vgll2a is required for neural crest cell survival during zebrafish craniofacial development. *Dev Biol* **357**, 269-281.

**Kameda, Y., Saitoh, T., Nemoto, N., Katoh, T., Iseki, S. and Fujimura, T.** (2013). Hes1 is required for the development of pharyngeal organs and survival of neural crest-derived mesenchymal cells in pharyngeal arches. *Cell Tissue Res* **353**, 9-25.

**Koo, B. K., Lim, H. S., Song, R., Yoon, M. J., Yoon, K. J., Moon, J. S., Kim, Y. W., Kwon, M. C., Yoo, K. W., Kong, M. P., et al.** (2005). Mind bomb 1 is essential for generating functional Notch ligands to activate Notch. *Development* **132**, 3459-3470.

**Kriebitz, N. N., Kiecker, C., McCormick, L., Lumsden, A., Graham, A. and Bell, E.** (2009). PRDC regulates placode neurogenesis in chick by modulating BMP signalling. *Dev Biol* **336**, 280-292.

**Kwan, C. T., Tsang, S. L., Krumlauf, R. and Sham, M. H.** (2001). Regulatory analysis of the mouse Hoxb3 gene: multiple elements work in concert to direct temporal and spatial patterns of expression. *Dev Biol* **232**, 176-190.

**Ladher, R. K., O'Neill, P. and Begbie, J.** (2010). From shared lineage to distinct functions: the development of the inner ear and epibranchial placodes. *Development* **137**, 1777-1785.

**Li, D., Sakuma, R., Vakili, N. A., Mo, R., Puviindran, V., Deimling, S., Zhang, X., Hopyan, S. and Hui, C. C.** (2014). Formation of proximal and anterior limb skeleton requires early function of Irx3 and Irx5 and is negatively regulated by Shh signaling. *Dev Cell* **29**, 233-240.

**Litsiou, A., Hanson, S. and Streit, A.** (2005). A balance of FGF, BMP and WNT signalling positions the future placode territory in the head. *Development* **132**, 4051-4062.

**Marklund, U., Hansson, E. M., Sundstrom, E., de Angelis, M. H., Przemeck, G. K., Lendahl, U., Muhr, J. and Ericson, J.** (2010). Domain-specific control of neurogenesis achieved through patterned regulation of Notch ligand expression. *Development* **137**, 437-445.

**McCabe, K. L. and Bronner-Fraser, M.** (2009). Molecular and tissue interactions governing induction of cranial ectodermal placodes. *Developmental Biology* **332**, 189-195.

**McCarroll, M. N., Lewis, Z. R., Culbertson, M. D., Martin, B. L., Kimelman, D. and Nechiporuk, A. V.** (2012). Graded levels of Pax2a and Pax8 regulate cell differentiation during sensory placode formation. *Development* **139**, 2740-2750.

**McCarroll, M. N. and Nechiporuk, A. V.** (2013). Fgf3 and Fgf10a work in concert to promote maturation of the epibranchial placodes in zebrafish. *PLoS One* **8**, e85087.
**Minoux, M. and Rijli, F. M.** (2010). Molecular mechanisms of cranial neural crest cell migration and patterning in craniofacial development. *Development* **137**, 2605-2621.
**Muller, F. and O'Rahilly, R.** (1988). The development of the human brain from a closed neural tube at stage 13. *Anat Embryol (Berl)* **177**, 203-224.
**Murtaugh, L. C., Stanger, B. Z., Kwan, K. M. and Melton, D. A.** (2003). Notch signaling controls multiple steps of pancreatic differentiation. *Proceedings of the National Academy of Sciences of the United States of America* **100**, 14920-14925.
**Ohtsuka, T., Ishibashi, M., Gradwohl, G., Nakanishi, S., Guillemot, F. and Kageyama, R.** (1999). Hes1 and Hes5 as notch effectors in mammalian neuronal differentiation. *EMBO J* **18**, 2196-2207.
**Ohyama, T. and Groves, A. K.** (2004a). Expression of mouse Foxi class genes in early craniofacial development. *Dev Dyn* **231**, 640-646.
**Ohyama, T. and Groves, A. K.** (2004b). Generation of Pax2-Cre mice by modification of a Pax2 bacterial artificial chromosome. *Genesis* **38**, 195-199.
**Rizzoti, K. and Lovell-Badge, R.** (2007). SOX3 activity during pharyngeal segmentation is required for craniofacial morphogenesis. *Development* **134**, 3437-3448.
**Roehl, H. and Nusslein-Volhard, C.** (2001). Zebrafish pea3 and erm are general targets of FGF8 signaling. *Curr Biol* **11**, 503-507.
**Saint-Jeannet, J. P. and Moody, S. A.** (2014). Establishing the pre-placodal region and breaking it into placodes with distinct identities. *Dev Biol* **389**, 13-27.
**Schlosser, G.** (2006). Induction and specification of cranial placodes. *Dev Biol* **294**, 303-351.
**Schlosser, G.** (2010). Making senses development of vertebrate cranial placodes. *Int Rev Cell Mol Biol* **283**, 129-234.
**Schlosser, G. and Ahrens, K.** (2004). Molecular anatomy of placode development in Xenopus laevis. *Dev Biol* **271**, 439-466.
**Siebel, C. and Lendahl, U.** (2017). Notch Signaling in Development, Tissue Homeostasis, and Disease. *Physiol Rev* **97**, 1235-1294.
**Sjoqvist, M. and Andersson, E. R.** (2019). Do as I say, Not(ch) as I do: Lateral control of cell fate. *Dev Biol* **447**, 58-70.
**Soriano, P.** (1999). Generalized lacZ expression with the ROSA26 Cre reporter strain. *Nat Genet* **21**, 70-71.
**Srinivas, S., Watanabe, T., Lin, C. S., William, C. M., Tanabe, Y., Jessell, T. M. and Costantini, F.** (2001). Cre reporter strains produced by targeted insertion of EYFP and ECFP into the ROSA26 locus. *BMC Dev Biol* **1**, 4.
**Streit, A.** (2002). Extensive cell movements accompany formation of the otic placode. *Dev Biol* **249**, 237-254.
**Streit, A.** (2004). Early development of the cranial sensory nervous system: from a common field to individual placodes. *Dev Biol* **276**, 1-15.
**Tripathi, V. B., Ishii, Y., Abu-Elmagd, M. M. and Scotting, P. J.** (2009). The surface ectoderm of the chick embryo exhibits dynamic variation in its response to neurogenic signals. *Int J Dev Biol* **53**, 1023-1033.
**Trokovic, N., Trokovic, R., Mai, P. and Partanen, J.** (2003). Fgfr1 regulates patterning of the pharyngeal region. *Genes Dev* **17**, 141-153.

**Urness, L. D., Bleyl, S. B., Wright, T. J., Moon, A. M. and Mansour, S. L.** (2011). Redundant and dosage sensitive requirements for Fgf3 and Fgf10 in cardiovascular development. *Dev Biol* **356**, 383-397.

**Urness, L. D., Paxton, C. N., Wang, X., Schoenwolf, G. C. and Mansour, S. L.** (2010). FGF signaling regulates otic placode induction and refinement by controlling both ectodermal target genes and hindbrain Wnt8a. *Dev Biol* **340**, 595-604.

**van Bueren, K. L., Papangeli, I., Rochais, F., Pearce, K., Roberts, C., Calmont, A., Szumska, D., Kelly, R. G., Bhattacharya, S. and Scambler, P. J.** (2010). Hes1 expression is reduced in Tbx1 null cells and is erequired for the development of structures affected in 22q11 deletion syndrome. *Dev Biol* **340**, 369-380.

**Verwoerd, C. D. and van Oostrom, C. G.** (1979). Cephalic neural crest and placodes. *Adv Anat Embryol Cell Biol* **58**, 1-75.

**Washausen, S. and Knabe, W.** (2013). Apoptosis contributes to placode morphogenesis in the posterior placodal area of mice. *Brain Structure and Function* **218**, 789-803.

**Washausen, S. and Knabe, W.** (2017). Pax2/Pax8-defined subdomains and the occurrence of apoptosis in the posterior placodal area of mice. *Brain Struct Funct* **222**, 2671-2695.

**Washausen, S. and Knabe, W.** (2018). Lateral line placodes of aquatic vertebrates are evolutionarily conserved in mammals. *Biol Open* **7**.

**Washausen, S., Obermayer, B., Brunnett, G., Kuhn, H. J. and Knabe, W.** (2005). Apoptosis and proliferation in developing, mature, and regressing epibranchial placodes. *Dev Biol* **278**, 86-102.

**Williams, R., Lendahl, U. and Lardelli, M.** (1995). Complementary and combinatorial patterns of Notch gene family expression during early mouse development. *Mech Dev* **53**, 357-368.

**Wright, T. J. and Mansour, S. L.** (2003). FGF signaling in ear development and innervation. *Curr Top Dev Biol* **57**, 225-259.

**Wu, J. Y. and Rao, Y.** (1999). Fringe: defining borders by regulating the notch pathway. *Curr Opin Neurobiol* **9**, 537-543.

**Xu, P. X., Zheng, W., Laclef, C., Maire, P., Maas, R. L., Peters, H. and Xu, X.** (2002). Eya1 is required for the morphogenesis of mammalian thymus, parathyroid and thyroid. *Development* **129**, 3033-3044.

**Zhang, H., Wang, L., Wong, E. Y. M., Tsang, S. L., Xu, P. X., Lendahl, U. and Sham, M. H.** (2017). An Eya1-Notch axis specifies bipotential epibranchial differentiation in mammalian craniofacial morphogenesis. *Elife* **6**, e30126

## Figures

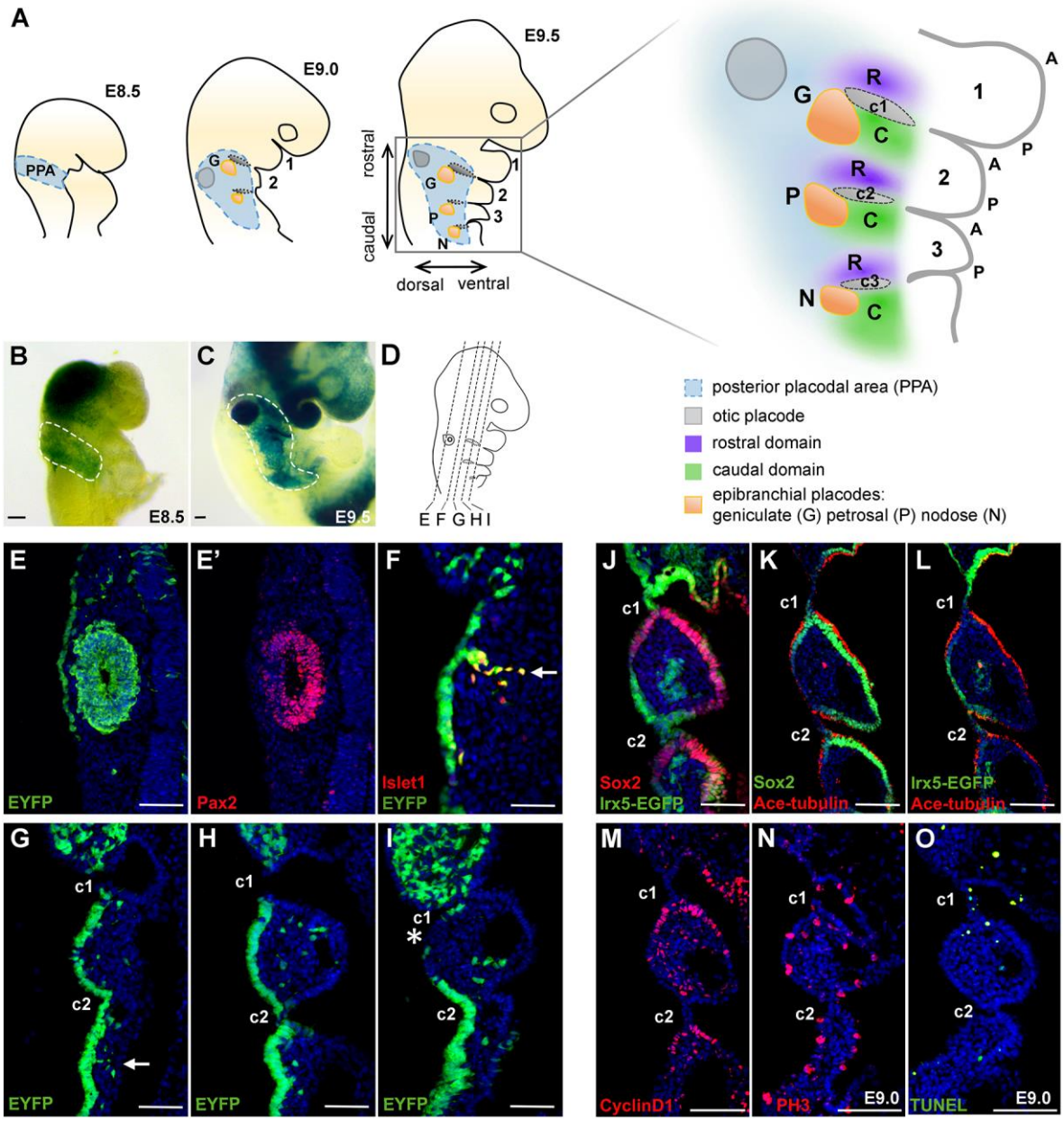


**Fig. 1. Analysis of epibranchial placodal cells derived from the posterior placodal area.** (A) Schematic diagram illustrating the locations of the posterior placodal area, the otic and epibranchial placode territories at E8.5, E9.0 and E9.5. The alignment of epibranchial placodal domains (rostral and caudal to each cleft) with the pharyngeal arches at E9.5 is illustrated. (B-C) Whole mount lacZ stained *Pax2Cre; R26R*$^{lacZ}$ embryos at (B) E8.5 (n=3) and (C) E9.5 (n=3). The dotted lines illustrate the PPA domain at E8.5 and otic/epibranchial domains at E9.5. (E-I) Immunostaining for

EYFP, Pax2 and Islet1 in serial coronal sections of an E9.5 *Pax2Cre; R26R*$^{EYFP}$ embryo from dorsal to ventral (n=3). The plane of sections are indicated as dashed lines in the diagram in (D). White arrows indicate positions of the delaminating neurons from geniculate (F) and petrosal (G) placodes. Asterisk (I) indicates the distal pharyngeal ectodermal cells. (J) Co-immunostaining of EGFP and Sox2 on E9.5 Irx5$^{EGFP/+}$ coronal sections (n=3). (K) Co-immunostaining of Sox2 and acetylated-tubulin on coronal section of E9.5 *WT* embryos (n=3). (L) Co-immunostaining of EGFP and acetylated-tubulin on coronal section of E9.5 *Irx5*$^{EGFP/+}$ embryos (n=3). (M) Immunostaining of CyclinD1 on coronal sections of E9.5 *WT* embryos (n=3). (N-O) Immunostaining of phospho-Histone H3 (PH3) (N) and TUNEL (O) on coronal section of E9.0 *WT* embryos (n=3). Scale bar = 100 μm; 1, 2, 3 indicate 1$^{st}$, 2$^{nd}$ and 3$^{rd}$ pharyngeal arch; c1, c2, c3 indicate 1$^{st}$, 2$^{nd}$ and 3$^{rd}$ pharyngeal cleft; A, anterior; P, posterior; R, rostral; C, caudal.

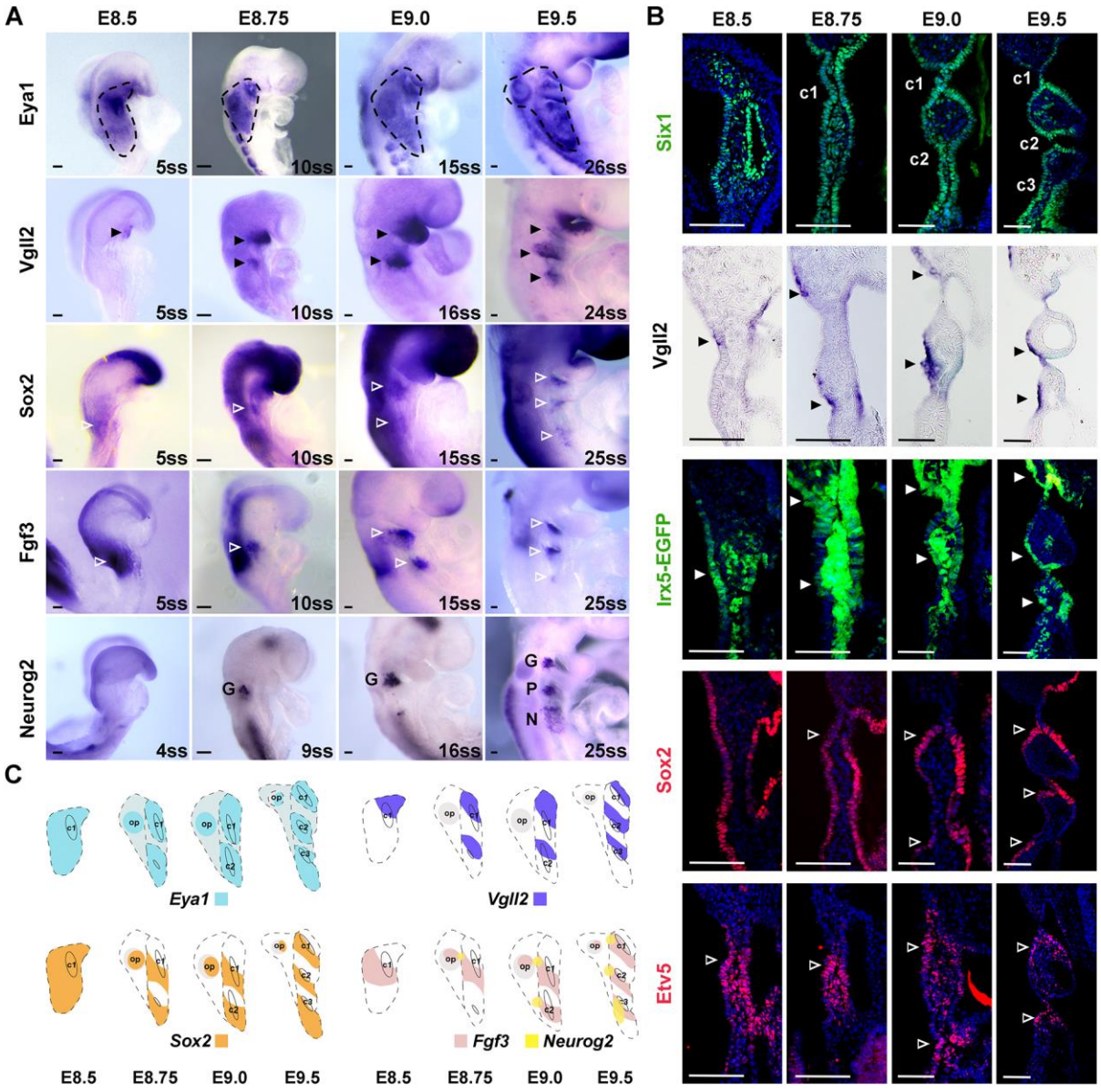


**Fig. 2. Spatiotemporal gene expression patterns during rostral and caudal regionalization of proximal pharyngeal ectoderm.** (A) Whole mount *in situ* hybridization of *WT* embryos from E8.5 to E9.5 with somite stages (ss) and genes as indicated (n≥3 for each stage and probe). The regions circled by black dotted lines indicate *Eya1*expression domain. (B) Immunostaining for Six1, Etv5 and Sox2 on coronal sections of *WT* embryos, immunostaining for EGFP on coronal sections of Irx5$^{EGFP/+}$ embryos, and coronal sections of *Vgll2* whole-mount *in situ* hybridized embryos from E8.5 to E9.5. Filled arrowheads indicate expression of Vgll2 (black) and Irx5 (white) in domains rostral to the clefts, open arrowheads indicate expression of Sox2, Fgf3 and Etv5 in domains caudal to the clefts. Scale bar = 100 μm. (C)

Schematic diagrams illustrating the expression regions of *Eya1* (circled by dotted line, blue), *Vgll2* (purple), *Sox2* (orange), *Fgf3* (pink) and *Neurog2* (yellow) during the specification of epibranchial placodes at indicated stages. op, otic placode; c1, c2, c3 indicate 1st, 2nd and 3rd pharyngeal cleft; G, geniculate placode; P, petrosal placode; N, nodose placode.

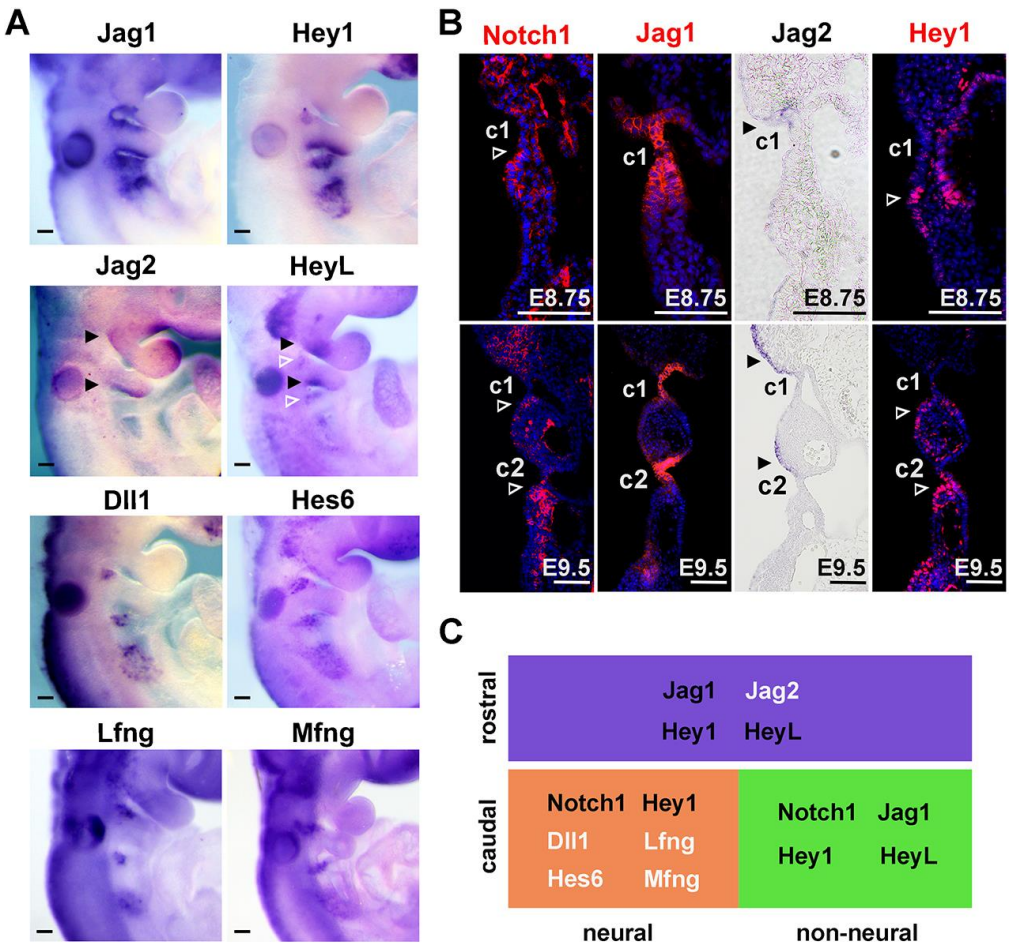


**Fig. 3. Regionalized expression of Notch signalling factors during posterior placodal area specification.** (A) Whole mount *In situ* hybridization showing *Jag1*, *Hey1*, *Jag2*, *HeyL*, *Dll1*, *Hes6*, *Lfng* and *Mfng* expression on *WT* embryos at E9.5 (n≥3 for each probe). (B) Coronal sections of *WT* embryos showing Notch1, Jag1, Hey1 and *Jag2* expression at E8.75 and E9.5. Scale bar = 100 μm. The black filled arrowheads indicate positive signals at domains rostral to the clefts; white open arrowheads indicate signals at domains caudal to the clefts. c1, c2 indicate 1st, and 2nd pharyngeal cleft. (C) Schematic diagram showing regionalized expression of distinct Notch factors at the rostral, non-neural caudal and neural dorsal-caudal domains.

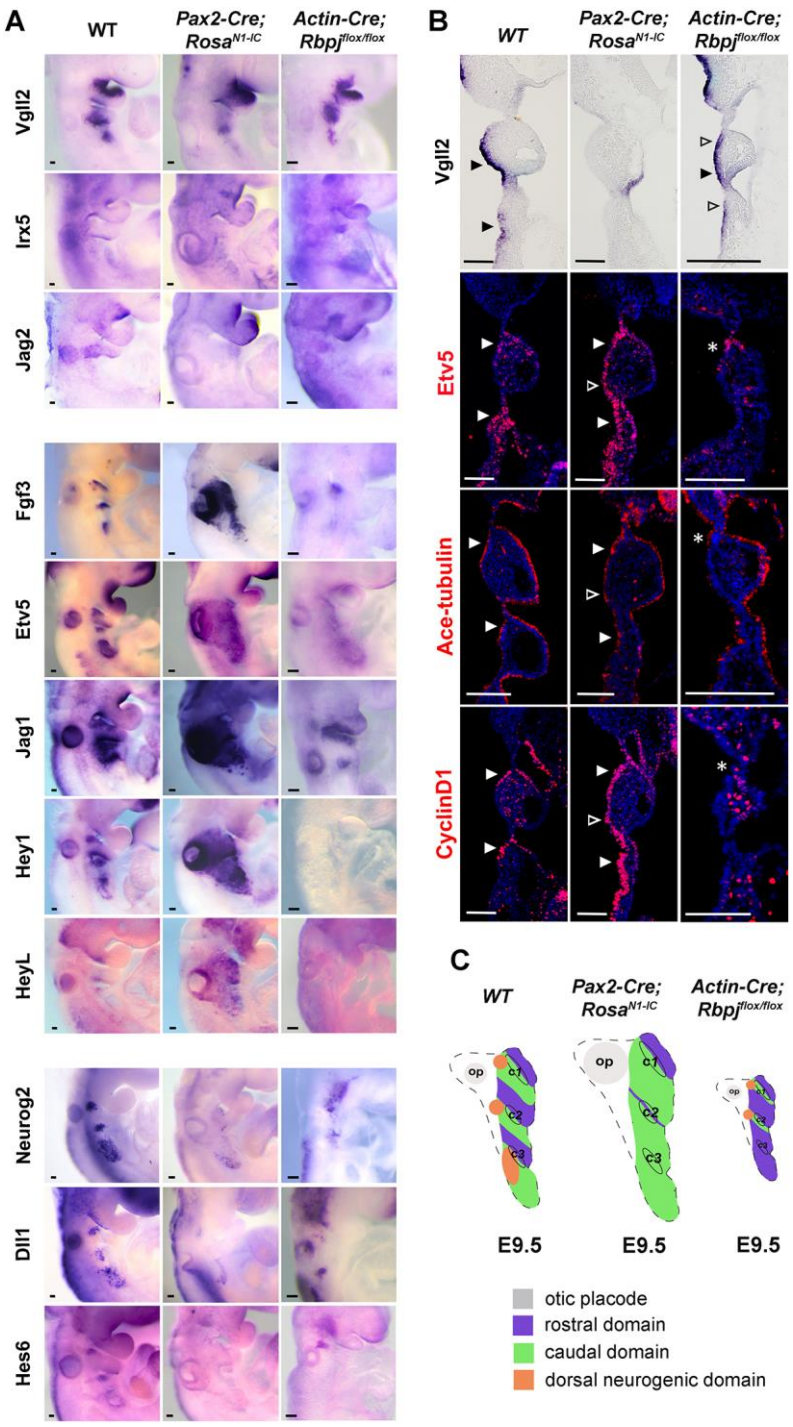


**Fig. 4. Expression of epibranchial placodal genes in Notch signaling mutants.** (A) Whole mount *in situ* hybridization showing *Vgll2, Irx5, Jag2, HeyL, Fgf3, Etv5, Jag1, Hey1, Neurog2, Dll1 and Hes6* expression on *WT, Pax2-cre;Rosa*$^{N1\text{-}IC}$ and *Actin-cre;Rbpj*$^{flox/flox}$ embryos (n=3 for each genotype and probe) at E9.5. (B) Coronal sections of *in situ* hybridized embryos showing *Vgll2* expression, and immunostaining of Etv5, acetylated-tubulin and CyclinD1 on coronal sections of embryos at E9.5 in

indicated genotypes (n=3 for each genotype and marker). Filled arrowheads represent normal expression domains, open arrowheads indicate ectopic expression domains. Asterisks indicate residual signals of indicated markers in pharyngeal ectoderm of *Actin-cre;Rbpj*$^{flox/flox}$ embryos. Scale bar = 100 µm. (C) Schematic summary of epibranchial placode rostral and caudal domain patterning phenotypes in gain-of-function and loss-of-function Notch mutant embryos at E9.5.

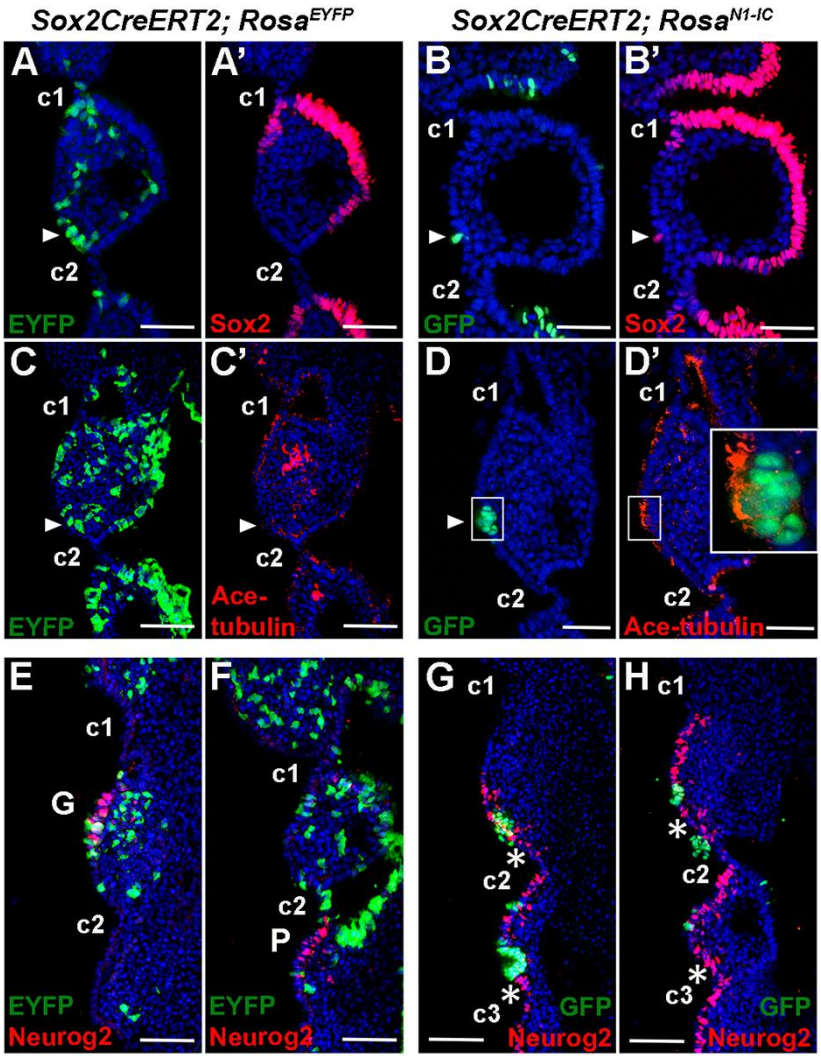


**Fig. 5. Analysis of pharyngeal epithelial markers in Notch1 gain-of-function mutant showing cell fate changes in the rostral epithelial domain.** (A-H) Immunostaining of EYFP, GFP, Sox2, Acetylated-tubulin and Neurog2 on coronal sections of *Sox2creERT2;Rosa*$^{EYFP}$ and *Sox2creERT2;Rosa*$^{N1\text{-}IC}$ (N1ICD is linked with IRES-GFP) embryos at E9.5 (n=3 for each genotype and markers). Scale bar = 100 µm. Tamoxifen was injected at E7.5, and the embryos examined at E9.5. Sox2-expressing caudal-like cells (B') and Neurog2+ pre-neural cells (G,H) were found in domains rostral to the clefts when Notch signalling is activated. c1, c2, c3 indicate 1$^{st}$, 2$^{nd}$ and 3$^{rd}$ pharyngeal cleft; arrowheads indicate EYFP+ or GFP+ (N1ICD+) cells in rostral domains; asterisks indicate ectopic Neurog2+ cells in domains rostral to the clefts. G, geniculate placode; P, petrosal placode.

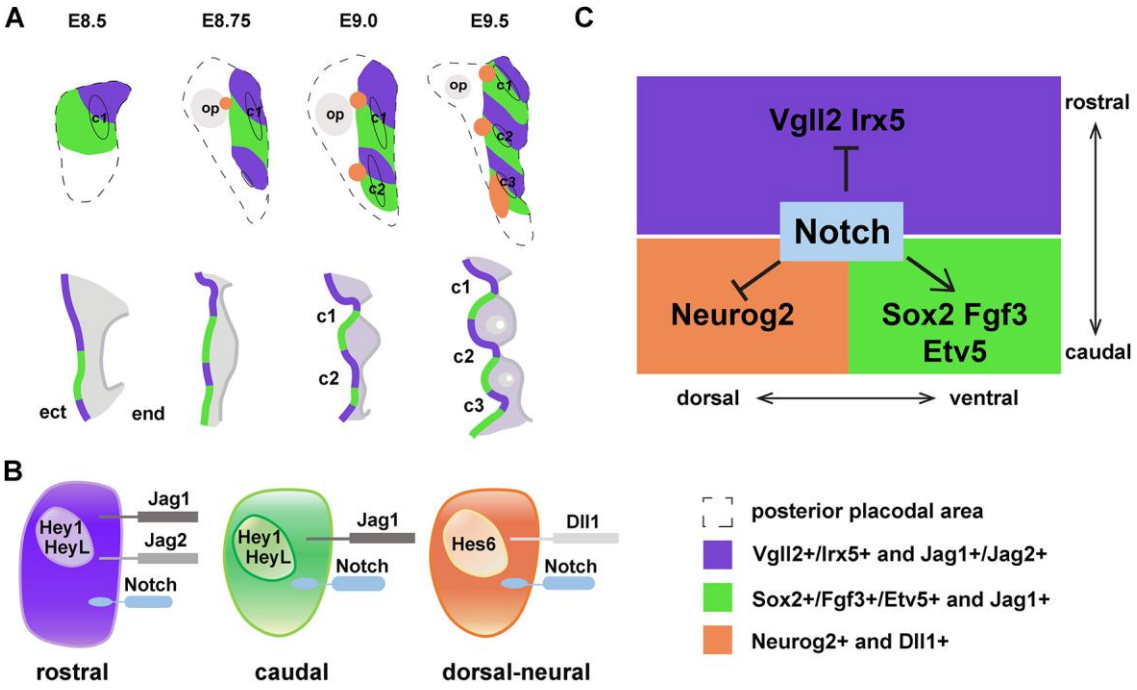


**Fig. 6. Model for how Notch signalling may regulate early rostral-caudal and dorsal-ventral regionalization of the epibranchial placode and proximal pharyngeal ectoderm.** (A) Stepwise segregation of posterior placodal area into geniculate, petrosal and nodose placodes (orange) as well as rostral (purple) and caudal (green) epibranchial epithelial domains from E8.5 to E9.5. The upper panel illustrates the sagittal view, while the lower panel depicts the coronal section view. Black oval lines indicate positions of pharyngeal clefts; dotted lines demarcate the posterior placodal area. c1, c2, c3 indicate the 1$^{st}$, 2$^{nd}$ and 3$^{rd}$ pharyngeal clefts; op, otic placode. (B) A schematic diagram illustrating the expression of Notch signalling factors in the rostral, caudal and dorsal-neural epibranchial placodal cells. (C) Proposed model for the role of Notch signalling in regulating regionalization and cell fates specification of the proximal pharyngeal ectodermal cells.

# Figure S1

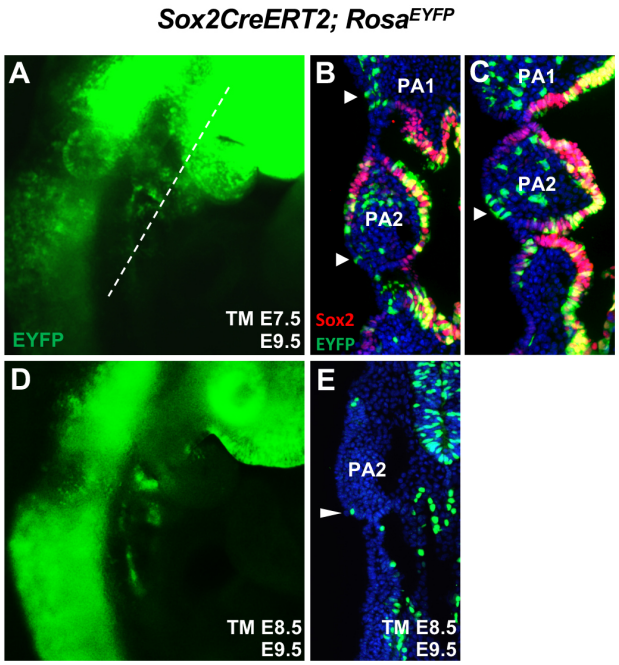


**Figure S1. Lineage tracing of the Sox2+ placodal precursors in *Sox2CreERT2; Rosa$^{EYFP}$* embryos at E9.5.** (A and D) Whole mount *EYFP* fluorescence at E9.5 after the tamoxifen (TM) injection at E7.5 (A) (n=4) and E8.5 (D) (n=2). (B, C and E) Coronal section of the E9.5 *Sox2CreERT2; Rosa$^{EYFP}$* embryos with tamoxifen injected at E7.5 (B and C) (n=4) and at E8.5 (E) (N=2). Arrows indicate the EYFP+ cells in pharyngeal ectoderm. PA, pharyngeal arch.

# Figure S2

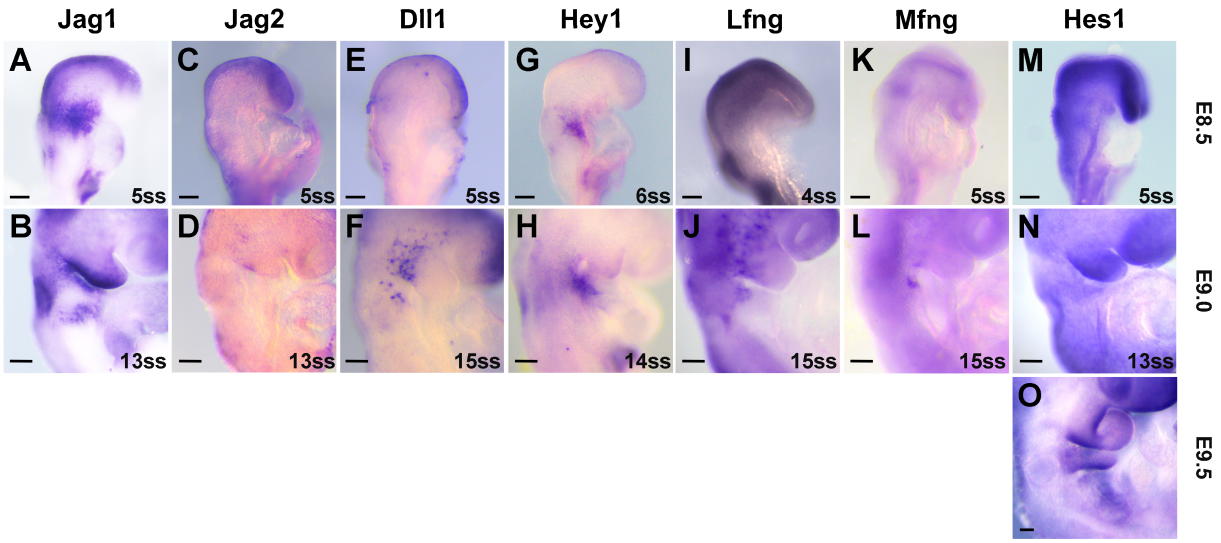


**Figure S2. Distinct expression of Notch signalling factors during the early stage of posterior placodal area specification.** (A-O) Whole mount In situ hybridization showing *Jag1* (A and B), *Jag2* (C and D), *Dll1* (E and F), *Hey1* (G and H), *Lfng* (I and J), *Mfng* (K and L) and *Hes1* (M-O) expression on WT embryos at indicated stages (n≥3 each stage).

# Figure S3

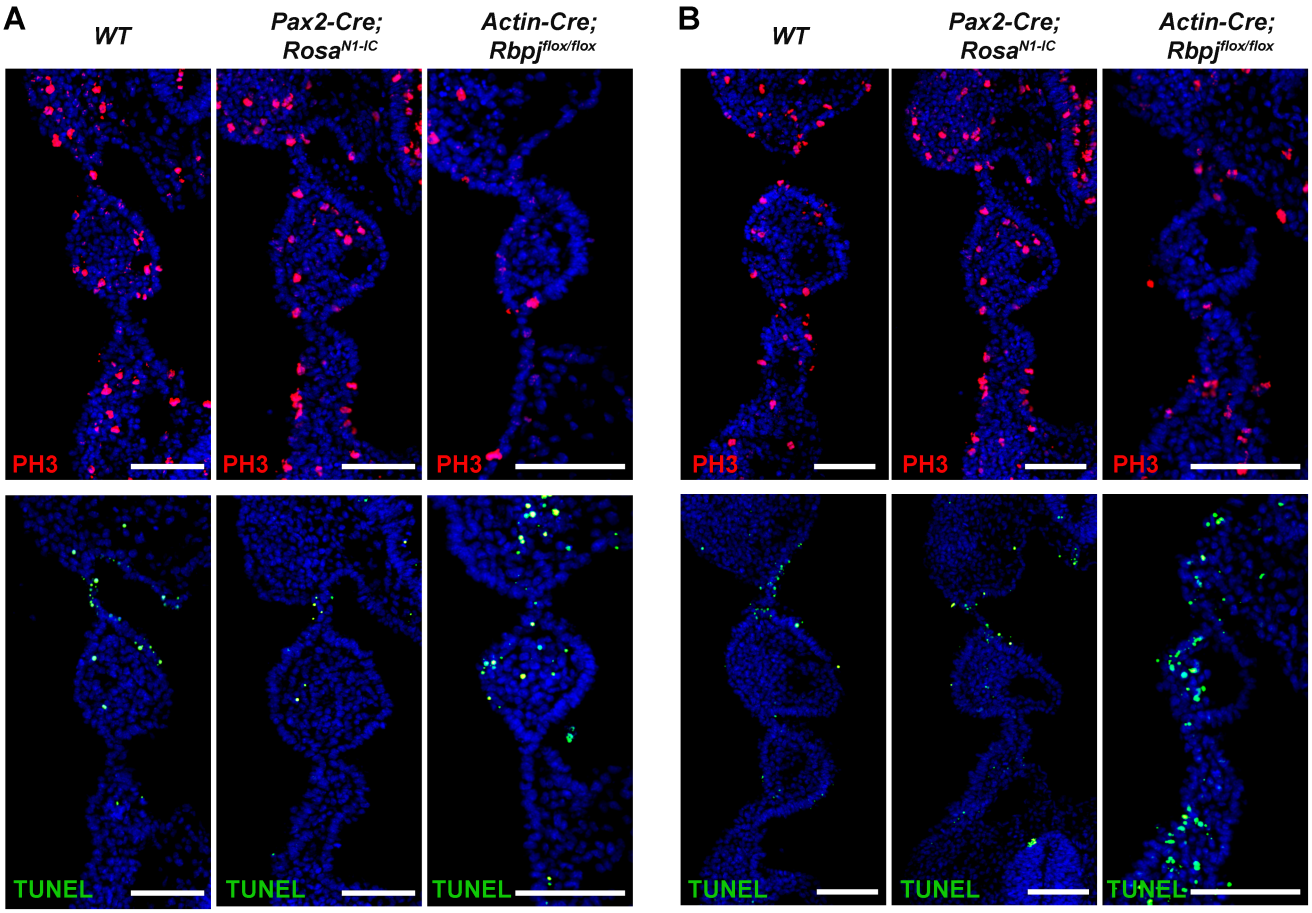


**Figure S3. Cell apoptosis and proliferation analysis on *WT*, *Pax2-Cre;Rosa$^{N1\text{-}IC}$* and *ActinCre;Rbpj$^{flox/flox}$* embryos.** (A and B) Immunostaining of phospho-histone H3 (PH3) and TUNEL on coronal sections of *WT*, *Pax2-Cre;Rosa$^{N1\text{-}IC}$* and *Actin-Cre;Rbpj$^{flox/flox}$* embryos at E9.0 (A) (n≥2) and E9.5 (B) (n=1). Scale bar = 100 µm.

## Supplementary Tables

### Table S1: Sequences of primers for genotyping of mouse lines

| Mouse line | Primer | Sequence |
|---|---|---|
| Cre | Forward (F) | 5' ACGGAAATCCATCGCTCGACCAGTT 3' |
| | Reverse (R) | 5' GTCCGGGCTGCCACGACCAA 3' |
| Irx5$^{+}$ | F | 5' GGTCCCGAAGGGCCAGAATCAGAATTGGGG 3' |
| | R | 5' GCATTCTTCCGGTACGCGGGGTCCCCATA 3' |
| Irx5$^{EGFP}$ | F | 5' GGTCCCGAAGGGCCAGAATCAGAATTGGGG 3' |
| | R | 5' CCGGTGGATGTGGAATGTGTGCGAGGCCA 3' |
| RBPJ$^{+}$ | F | 5' GTTCTTAACCTGTTGGTCGGAACC 3' |
| | R | 5' GCTTGAGGCTTGATGTTCTGTATTGC 3' |
| RBPJ$^{flox}$ | F | 5' GTTCTTAACCTGTTGGTCGGAACC 3' |
| | R | 5' GCAATCCATCTTGTTCAATGGCC 3' |
| RBPJ$^{-}$ | F | 5' GCTTGAGGCTTGATGTTCTGTATTGC 3' |
| | R | 5' CTGAGTAAGATGAGATGCTGACATCTGA 3' |
| Rosa$^{N1\text{-}IC}$ | F | 5' ACCCTGGACTACTGCGCCC 3' |
| | R | 5' CGAAGAGTTTGTCCTCAACCG 3' |

### Table S2: Sequences of primers for cDNA cloning

| cDNA | Forward | Reverse |
|---|---|---|
| Dll1 | 5' ATCTGTCTGCCAGGG 3' | 5' GCACCGTTAGAACAA 3' |
| Hes6 | 5' AGTAGTTTGCACTAG 3' | 5' AGAACCTCGGCGTTC 3' |
| Hey1 | 5' ATGAAGAGAGCTCAC 3' | 5' TTAGAAAGCTCCGAT 3' |
| HeyL | 5' AGTATTGGGTTTCGG 3' | 5' TGATTTCTGAGACCC 3' |
| Mfng | 5' AGCTGGTGCGGTTCT 3' | 5' ATCCCCTCCCACACA 3' |
| Vgll2 | 5' TCCTCATTTTCCAAC 3' | 5' TAGGCAGAGGCTTGT 3' |

### Table S3: Probes for in situ hybridization

| Probes | Restriction enzyme for anti-sense probe | Polymerase for transcription | Reference |
|---|---|---|---|
| Dll1 | BamHI | T7 | this study |
| Eya1 | SalI | T7 | Xu et al., 1997 |
| Etv5 | HindIII | T3 | Kindly provided by Frank Costantini |
| Fgf3 | SalI | T7 | Wilkinson et al., 1988 |
| Hes6 | BamHI | T7 | this study |
| Hes1 | EcoRI | T7 | Zheng et al., 2000 |
| Hey1 | BamHI | T7 | this study |
| HeyL | BamHI | T7 | this study |
| Jag1 | EcoRI | T3 | Mitsiadis et al., 1997 |
| Lfng | HindIII | T7 | Zhang et al., 1998 |

| | | | |
|---|---|---|---|
| Mfng | BamHI | T7 | this study |
| Neurog2 | BamHI | T7 | Gradwohl et al., 1996 |
| Notch1 | Apa1 | SP6 | Williams et al., 1995b |
| Six1 | BamHI | T3 | Oliver et al., 1995 |
| Sox2 | AccI | T3 | Avilion et al., 2003 |
| Vgll2 | BamHI | T7 | this study |

**Table S4: Antibodies used for immunohistochemistry**

| Antibodies | Source | Identifiers | Dilutions |
|---|---|---|---|
| Donkey anti-Rabbit IgG (H+L) Highly Cross-Adsorbed Secondary Antibody, Alexa Fluor 488 | Thermo Fisher Scientific | A21206, RRID:AB_2535792 | 1:500 |
| Goat polyclonal anti-Notch1 (C20) | Santa Cruz Biotechnology | sc-6014, RRID: AB_650336 | 1:400 |
| Goat polyclonal anti-Sox2 | Neuromics | GT15098-100, RRID:AB_21955800 | 1:500 |
| Mouse monoclonal anti-Acetylated-tubulin | Sigma-Aldrich | T7451, RRID:AB_609894 | 1:700 |
| Mouse monoclonal anti-Neurog2 | R&D systems | MAB3314, RRID:AB_2149520 | 1:1000 |
| Mouse polyclonal anti-Islet1 | DSHB | PCRP-ISL1-1A9, RRID:AB_2618775 | 1:400 |
| Rabbit polyclonal anti-GFP | Abcam | ab6556, RRID:AB_305564 | 1:1000 |
| Rabbit polyclonal anti-Hey1 | Abcam | AB22614, RRID:AB_447195 | 1:500 |
| Rabbit polyclonal anti-Pax2 | Invitrogen | 71-6000, RRID:AB_2533990 | 1:500 |
| Rabbit polyclonal anti-Six1 | Sigma-Aldrich | HPA001893, RRID:AB_1079991 | 1:500 |
| Rat monoclonal anti-Jagged1 | DSHB | Ts1.15h, RRID: AB_528317 | 1:300 |
| Rabbit monoclonal anti-CyclinD1 | Abcam | ab16663 RRID: AB_443423 | 1:300 |
| Rabbit polyclonal anti-phospho-Histone H3 (Ser10) | Upstate | 06-570 RRID: AB_310177 | 1:500 |
| Sheep polyclonal anti-Digoxigenin-alkaline phosphatase | Sigma-Aldrich | Cat#11093274910 | 1:2000 |
| In Situ Cell Death Detection Kit, Fluorescein | Roche | Cat#11684795910 | NA |

## Supplementary References

**Avilion, A. A., Nicolis, S. K., Pevny, L. H., Perez, L., Vivian, N. and Lovell-Badge, R.** (2003). Multipotent cell lineages in early mouse development depend on SOX2 function. *Genes & development* **17**, 126-140.

**Gradwohl, G., Fode, C. and Guillemot, F.** (1996). Restricted expression of a novel murineatonal-related bHLH protein in undifferentiated neural precursors. *Developmental biology* **180**, 227-241.

**Mitsiadis, T. A., Henrique, D., Thesleff, I. and Lendahl, U.** (1997). Mouse Serrate-1 (Jagged-1): expression in the developing tooth is regulated by epithelial-mesenchymal interactions and fibroblast growth factor-4. *Development* **124**, 1473-1483.

**Oliver, G., Wehr, R., Jenkins, N. A., Copeland, N. G., Cheyette, B. N., Hartenstein, V., Zipursky, S. L. and Gruss, P.** (1995). Homeobox genes and connective tissue patterning. *Development* **121**, 693-705.

**Wilkinson, D. G., Peters, G., Dickson, C. and McMahon, A. P.** (1988). Expression of the FGF-related proto-oncogene int-2 during gastrulation and neurulation in the mouse. *The EMBO journal* **7**, 691-695.

**Williams, R., Lendahl, U. and Lardelli, M.** (1995). Complementary and combinatorial patterns of Notch gene family expression during early mouse development. *Mechanisms of development* **53**, 357-368.

**Xu, P.-X., Woo, I., Her, H., Beier, D. R. and Maas, R. L.** (1997). Mouse Eya homologues of the Drosophila eyes absent gene require Pax6 for expression in lens and nasal placode. *Development* **124**, 219-231.

**Zhang, N. and Gridley, T.** (1998). Defects in somite formation in lunatic fringe-deficient mice. *Nature* **394**, 374.

**Zheng, J. L., Shou, J., Guillemot, F., Kageyama, R. and Gao, W.-Q.** (2000). Hes1 is a negative regulator of inner ear hair cell differentiation. *Development* **127**, 4551-4560.

# Figure S1

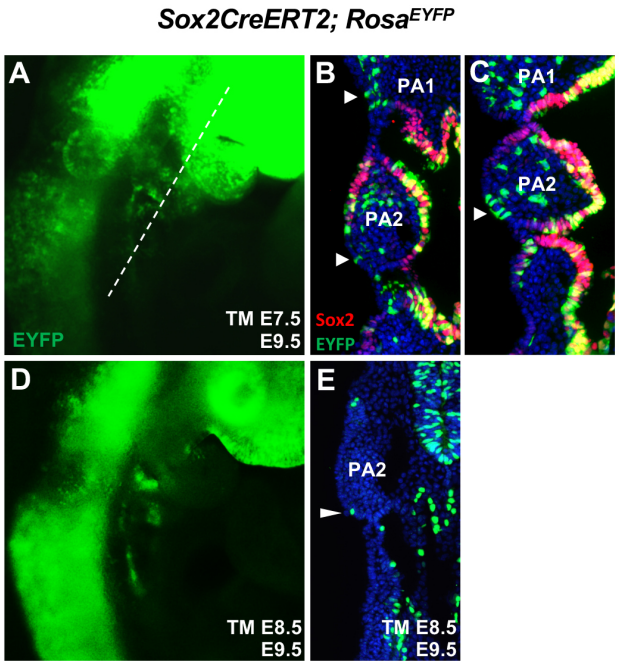


**Figure S1. Lineage tracing of the Sox2+ placodal precursors in *Sox2CreERT2; Rosa$^{EYFP}$* embryos at E9.5.** (A and D) Whole mount *EYFP* fluorescence at E9.5 after the tamoxifen (TM) injection at E7.5 (A) (n=4) and E8.5 (D) (n=2). (B, C and E) Coronal section of the E9.5 *Sox2CreERT2; Rosa$^{EYFP}$* embryos with tamoxifen injected at E7.5 (B and C) (n=4) and at E8.5 (E) (N=2). Arrows indicate the EYFP+ cells in pharyngeal ectoderm. PA, pharyngeal arch.

# Figure S2

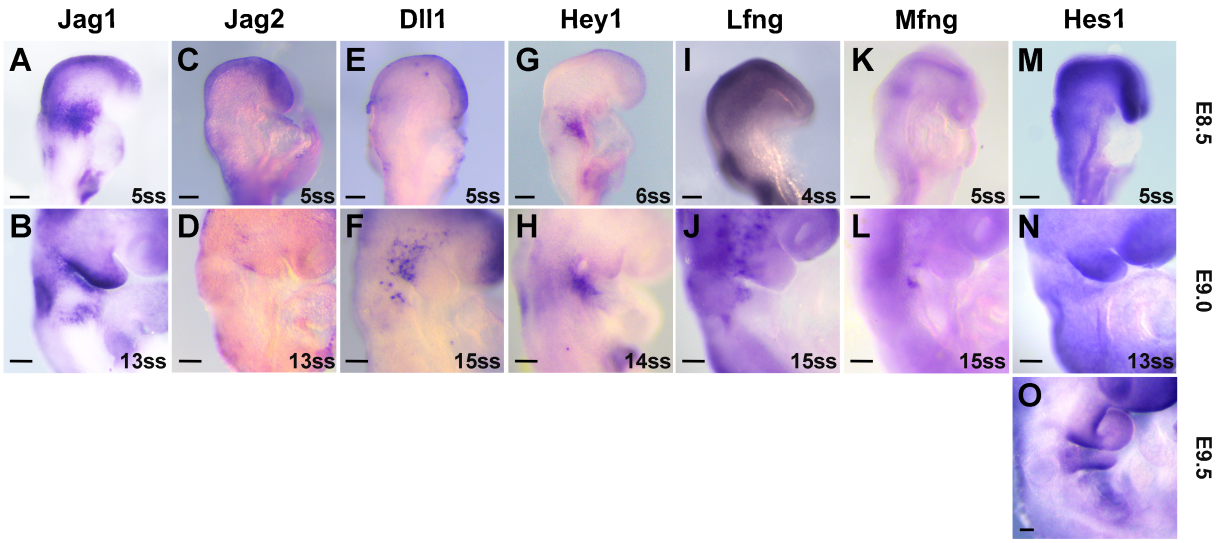


**Figure S2. Distinct expression of Notch signalling factors during the early stage of posterior placodal area specification.** (A-O) Whole mount In situ hybridization showing *Jag1* (A and B), *Jag2* (C and D), *Dll1* (E and F), *Hey1* (G and H), *Lfng* (I and J), *Mfng* (K and L) and *Hes1* (M-O) expression on WT embryos at indicated stages (n≥3 each stage).

# Figure S3

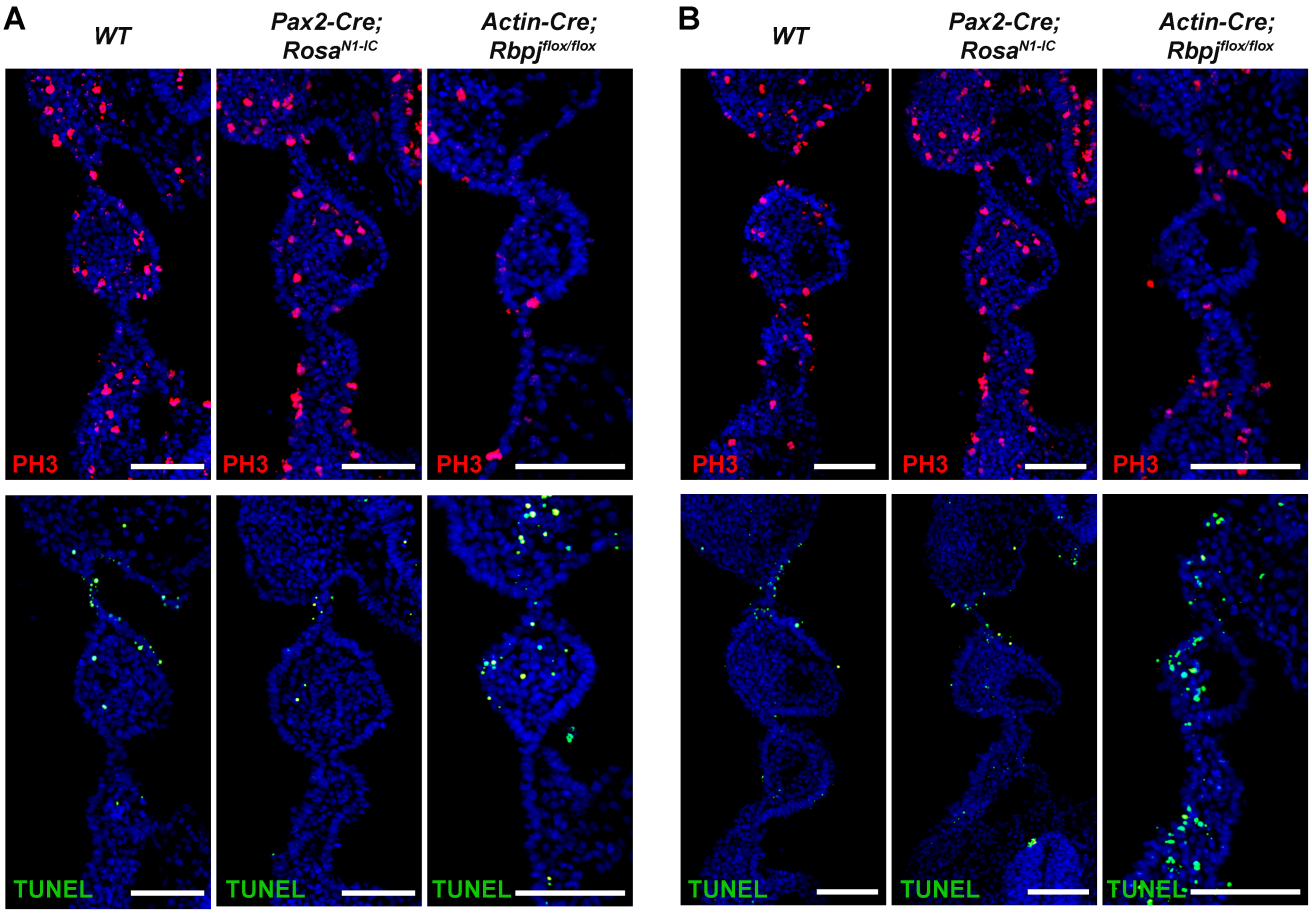


**Figure S3. Cell apoptosis and proliferation analysis on *WT*, *Pax2-Cre;Rosa$^{N1-IC}$* and *ActinCre;Rbpj$^{flox/flox}$* embryos.** (A and B) Immunostaining of phospho-histone H3 (PH3) and TUNEL on coronal sections of *WT*, *Pax2-Cre;Rosa$^{N1-IC}$* and *Actin-Cre;Rbpj$^{flox/flox}$* embryos at E9.0 (A) (n≥2) and E9.5 (B) (n=3). Scale bar = 100 µm.

## Supplementary Tables

### Table S1: Sequences of primers for genotyping of mouse lines

| Mouse line | Primer | Sequence |
|---|---|---|
| Cre | Forward (F) | 5' ACGGAAATCCATCGCTCGACCAGTT 3' |
| | Reverse (R) | 5' GTCCGGGCTGCCACGACCAA 3' |
| Irx5$^{+}$ | F | 5' GGTCCCGAAGGGCCAGAATCAGAATTGGGG 3' |
| | R | 5' GCATTCTTCCGGTACGCGGGGTCCCCATA 3' |
| Irx5$^{EGFP}$ | F | 5' GGTCCCGAAGGGCCAGAATCAGAATTGGGG 3' |
| | R | 5' CCGGTGGATGTGGAATGTGTGCGAGGCCA 3' |
| RBPJ$^{+}$ | F | 5' GTTCTTAACCTGTTGGTCGGAACC 3' |
| | R | 5' GCTTGAGGCTTGATGTTCTGTATTGC 3' |
| RBPJ$^{flox}$ | F | 5' GTTCTTAACCTGTTGGTCGGAACC 3' |
| | R | 5' GCAATCCATCTTGTTCAATGGCC 3' |
| RBPJ$^{-}$ | F | 5' GCTTGAGGCTTGATGTTCTGTATTGC 3' |
| | R | 5' CTGAGTAAGATGAGATGCTGACATCTGA 3' |
| Rosa$^{N1\text{-}IC}$ | F | 5' ACCCTGGACTACTGCGCCC 3' |
| | R | 5' CGAAGAGTTTGTCCTCAACCG 3' |

### Table S2: Sequences of primers for cDNA cloning

| cDNA | Forward | Reverse |
|---|---|---|
| Dll1 | 5' ATCTGTCTGCCAGGG 3' | 5' GCACCGTTAGAACAA 3' |
| Hes6 | 5' AGTAGTTTGCACTAG 3' | 5' AGAACCTCGGCGTTC 3' |
| Hey1 | 5' ATGAAGAGAGCTCAC 3' | 5' TTAGAAAGCTCCGAT 3' |
| HeyL | 5' AGTATTGGGTTTCGG 3' | 5' TGATTTCTGAGACCC 3' |
| Mfng | 5' AGCTGGTGCGGTTCT 3' | 5' ATCCCCTCCCACACA 3' |
| Vgll2 | 5' TCCTCATTTTCCAAC 3' | 5' TAGGCAGAGGCTTGT 3' |

### Table S3: Probes for in situ hybridization

| Probes | Restriction enzyme for anti-sense probe | Polymerase for transcription | Reference |
|---|---|---|---|
| Dll1 | BamHI | T7 | this study |
| Eya1 | SalI | T7 | Xu et al., 1997 |
| Etv5 | HindIII | T3 | Kindly provided by Frank Costantini |
| Fgf3 | SalI | T7 | Wilkinson et al., 1988 |
| Hes6 | BamHI | T7 | this study |
| Hes1 | EcoRI | T7 | Zheng et al., 2000 |
| Hey1 | BamHI | T7 | this study |
| HeyL | BamHI | T7 | this study |
| Jag1 | EcoRI | T3 | Mitsiadis et al., 1997 |
| Lfng | HindIII | T7 | Zhang et al., 1998 |

| | | | |
|---|---|---|---|
| Mfng | BamHI | T7 | this study |
| Neurog2 | BamHI | T7 | Gradwohl et al., 1996 |
| Notch1 | Apa1 | SP6 | Williams et al., 1995b |
| Six1 | BamHI | T3 | Oliver et al., 1995 |
| Sox2 | AccI | T3 | Avilion et al., 2003 |
| Vgll2 | BamHI | T7 | this study |

**Table S4: Antibodies used for immunohistochemistry**

| Antibodies | Source | Identifiers | Dilutions |
|---|---|---|---|
| Donkey anti-Rabbit IgG (H+L) Highly Cross-Adsorbed Secondary Antibody, Alexa Fluor 488 | Thermo Fisher Scientific | A21206, RRID:AB_2535792 | 1:500 |
| Goat polyclonal anti-Notch1 (C20) | Santa Cruz Biotechnology | sc-6014, RRID: AB_650336 | 1:400 |
| Goat polyclonal anti-Sox2 | Neuromics | GT15098-100, RRID:AB_21955800 | 1:500 |
| Mouse monoclonal anti-Acetylated-tubulin | Sigma-Aldrich | T7451, RRID:AB_609894 | 1:700 |
| Mouse monoclonal anti-Neurog2 | R&D systems | MAB3314, RRID:AB_2149520 | 1:1000 |
| Mouse polyclonal anti-Islet1 | DSHB | PCRP-ISL1-1A9, RRID:AB_2618775 | 1:400 |
| Rabbit polyclonal anti-GFP | Abcam | ab6556, RRID:AB_305564 | 1:1000 |
| Rabbit polyclonal anti-Hey1 | Abcam | AB22614, RRID:AB_447195 | 1:500 |
| Rabbit polyclonal anti-Pax2 | Invitrogen | 71-6000, RRID:AB_2533990 | 1:500 |
| Rabbit polyclonal anti-Six1 | Sigma-Aldrich | HPA001893, RRID:AB_1079991 | 1:500 |
| Rat monoclonal anti-Jagged1 | DSHB | Ts1.15h, RRID: AB_528317 | 1:300 |
| Rabbit monoclonal anti-CyclinD1 | Abcam | ab16663 RRID: AB_443423 | 1:300 |
| Rabbit polyclonal anti-phospho-Histone H3 (Ser10) | Upstate | 06-570 RRID: AB_310177 | 1:500 |
| Sheep polyclonal anti-Digoxigenin-alkaline phosphatase | Sigma-Aldrich | Cat#11093274910 | 1:2000 |
| In Situ Cell Death Detection Kit, Fluorescein | Roche | Cat#11684795910 | NA |

## Supplementary References

**Avilion, A. A., Nicolis, S. K., Pevny, L. H., Perez, L., Vivian, N. and Lovell-Badge, R.** (2003). Multipotent cell lineages in early mouse development depend on SOX2 function. *Genes & development* **17**, 126-140.

**Gradwohl, G., Fode, C. and Guillemot, F.** (1996). Restricted expression of a novel murineatonal-related bHLH protein in undifferentiated neural precursors. *Developmental biology* **180**, 227-241.

**Mitsiadis, T. A., Henrique, D., Thesleff, I. and Lendahl, U.** (1997). Mouse Serrate-1 (Jagged-1): expression in the developing tooth is regulated by epithelial-mesenchymal interactions and fibroblast growth factor-4. *Development* **124**, 1473-1483.

**Oliver, G., Wehr, R., Jenkins, N. A., Copeland, N. G., Cheyette, B. N., Hartenstein, V., Zipursky, S. L. and Gruss, P.** (1995). Homeobox genes and connective tissue patterning. *Development* **121**, 693-705.

**Wilkinson, D. G., Peters, G., Dickson, C. and McMahon, A. P.** (1988). Expression of the FGF-related proto-oncogene int-2 during gastrulation and neurulation in the mouse. *The EMBO journal* **7**, 691-695.

**Williams, R., Lendahl, U. and Lardelli, M.** (1995). Complementary and combinatorial patterns of Notch gene family expression during early mouse development. *Mechanisms of development* **53**, 357-368.

**Xu, P.-X., Woo, I., Her, H., Beier, D. R. and Maas, R. L.** (1997). Mouse Eya homologues of the Drosophila eyes absent gene require Pax6 for expression in lens and nasal placode. *Development* **124**, 219-231.

**Zhang, N. and Gridley, T.** (1998). Defects in somite formation in lunatic fringe-deficient mice. *Nature* **394**, 374.

**Zheng, J. L., Shou, J., Guillemot, F., Kageyama, R. and Gao, W.-Q.** (2000). Hes1 is a negative regulator of inner ear hair cell differentiation. *Development* **127**, 4551-4560.